Acta Oceanol. Sin., 2021, Vol. 40, No. 2, P. 13–28
https://doi.org/10.1007/s13131-021-1757-7
http://www.hyxb.org.cn
E-mail: hyxbe@263.net

Reinterpretation of the northern South China Sea pre-Cenozoic basement and geodynamic implications of the South China continent: constraints from combined geological and geophysical records

Weilin Zhu[1], Yuchi Cui[1, 2]*, Lei Shao[1]*, Peijun Qiao[1], Peng Yu[1], Jianxiang Pei[3], Xinyu Liu[3], Hao Zhang[1]

[1] State Key Laboratory of Marine Geology, Tongji University, Shanghai 200092, China

[2] The Institute for Geoscience Research (TIGeR), School of Earth and Planetary Sciences, Curtin University, Perth 6845, Australia

[3] Hainan Energy Co., Ltd., CNOOC, Haikou 570145, China

Received 20 November 2019; accepted 3 June 2020

Abstract

The pre-Cenozoic northern South China Sea (SCS) Basin basement was supposed to exist as a complex of heterogeneous segments, divided by dozens of N–S faulting. Unfortunately, only the Hainan Island and the northeastern SCS region were modestly dated while the extensive basement remains roughly postulated by limited geophysical data. This study presents a systematic analysis including U-Pb geochronology, elemental geochemistry and petrographic identification on granite and meta-clastic borehole samples from several key areas. Constrained from gravity-magnetic joint inversion, this interpretation will be of great significance revealing the tectono-magmatic evolution along the southeastern margin of the Eurasian Plate. Beneath the thick Cenozoic sediments, the northern SCS is composed of a uniform Mesozoic basement while the Precambrian rocks are only constricted along the Red River Fault Zone. Further eastern part of the northern SCS below the Cenozoic succession was widely intruded by granites with Jurassic-to-early Cretaceous ages. Further western part, on the other hand, is represented by meta-sedimentary rocks with relatively sporadic granite complexes. To be noted, the western areas derived higher-degree and wider metamorphic zones, which is in contrast with the lower-degree and narrower metamorphic belt developed in the eastern region. Drastic collisions between the Indochina Block and South China continent took place since at least late Triassic, resulting in large-scale suturing and deformation zones. At the westernmost part of the northern SCS, the intracontinental amalgamation with closure of the Meso-Tethys has caused fairly stronger and broader metamorphism. One metamorphic biotite granite is located on the suturing belt and yields a Precambrian U-Pb age. It likely represents the relict from the ancient Gondwana supercontinent or its fringes. Arc-continental collision between the Paleo-Pacific and the southeast China Block, on the other hand, results in a relatively narrow NE–SW trending metamorphic belt during the late Mesozoic. Within the overall geological setting, the Cenozoic SCS oceanic basin was subsequently generated from a series of rifting and faulting processes along the collisional-accretionary continental margin.

Key words: South China Sea, pre-Cenozoic basement, U-Pb geochronology, Paleo-Pacific subduction, intracontinental collision, metamorphic belt

Citation: Zhu Weilin, Cui Yuchi, Shao Lei, Qiao Peijun, Yu Peng, Pei Jianxiang, Liu Xinyu, Zhang Hao. 2021. Reinterpretation of the northern South China Sea pre-Cenozoic basement and geodynamic implications of the South China continent: constraints from combined geological and geophysical records. Acta Oceanologica Sinica, 40(2): 13–28, doi: 10.1007/s13131-021-1757-7

1 Introduction

The South China Sea (SCS) is the largest marginal sea within the western Pacific. Extensive investigations have been conducted on the SCS, including scientific and industrial drilling, dredging, and multiple-channel seismic profiles. These surveys have significantly refined the understandings on the origin and subsequent opening of the SCS (Briais et al., 1993; Hsu et al., 2004; Franke et al., 2011; Barckhausen et al., 2014). In particular, recent International Ocean Drilling Program expeditions revealed that the northern SCS margin was neither completely "magma-rich" nor "magma-poor" identified in the other North Atlantic magmatism models (Larsen et al., 2018). Instead, the northern SCS is a representative of hyperextended margin, which is now considered as a missing link between "magma-rich" and "magma-poor" margins (Lei and Ren, 2016; Lei et al., 2019a). In order to precisely evaluate the Cenozoic tectonic evolution of the SCS, researches are also urged to be underpinned from the pre-Cenozoic framework and the geological processes which have greatly controlled the following Cenozoic evolutionary events. Beneath the Cenozoic sedimentary layer, the SCS Basin basement study is of crucial significance in structural geology and regional geodynamic reconstruction (Nissen et al., 1995a, 1995b;

Foundation item: The National Natural Science Foundation of China under contract Nos 42076066, 92055203 and 41874076; the National Science and Technology Major Project under contract Nos 2016ZX05026004-002 and 2017ZX05026005-005; the Fund of China Association for Science and Technology under contract No. 2018CASRQNJL18.
*Corresponding author, E-mail: cuiyuchi@tongji.edu.cn; lshao@tongji.edu.cn

Braitenberg et al., 2006). However, ages and properties of the pre-Cenozoic basement still require accurate geological evidence to improve interpretation and integrated reviews of previous studies (Fig. 1a).

Antecedent attempted to illustrate the formation and composition of the SCS Basin basement were based on sketchy petrographic description as well as insufficient geochronological data. Particularly, the wide underlying components of Yinggehai Basin and Qiongdongnan Basin still were proved to be fairly problematic and poorly explored (Pigott and Ru, 1994; Braitenberg et al., 2006; Franke et al., 2011; Pichot et al., 2014). Their onshore continental margins were identified with Proterozoic schists and gneiss, Paleozoic and Mesozoic metaclastic rocks, carbonates and volcanic rocks (Sun et al., 2014). For the seaward extension, this offshore part is even harder to trace due to scarce borehole penetration and lacking of precise dating analyses. It was extrapolated that the Yinggehai and Qiongdongnan Basin basements might have generated similar lithological and tectonic features to the northern Indochina Block margin (Nielsen et al., 1999). This assumption is in the light of basement consolidation during the collision and convergence between major continental blocks and scattered micro-terranes (Carter et al., 2001; Lepvrier et al., 2004; Li et al., 2006). According to previous studies, the onshore pre-Cenozoic meta-sedimentary strata and magmatic arc were likely to extend from land to sea. In some areas of Qiongdongnan Basin, the well-stratified formations are Mesozoic low-grade metamorphic sedimentary rocks (Nielsen et al., 1999). In the other sections, Precambrian metamorphic complexes were only restricted within continental shelf basement proximal to Vietnam (Hutchison, 1989; Dien, 1998). However, the low-resolution seismic profiles caused these considerations to remain uncertain. Upper Paleozoic carbonate platform deposits were also sporadically developed from the coastal region, such as the Beibu Gulf Basin and areas through the continental interior (Fyhn et al., 2018) (Fig. 1a). Tectonically, this heterogeneous Paleozoic-Mesozoic basement surrounding the Hainan Island seems to be mainly controlled from a NW–SE fault system (Sun et al., 2014). These early discoveries have led to a series of questions on the overall assessment of the pre-Cenozoic SCS Basin basement regarding its physical properties and distribution patterns. Under which type of geodynamic background was the basement generalized? How did the basement control or influence the subsequent rifting of the Cenozoic SCS basins?

Along the South China Block southeastern margin, the broad distribution of granitic and granodioritic magmatic records show that an Andean-type active continental margin has already existed from late Triassic or early Jurassic, to Cretaceous (Zhou and Li, 2000; Li and Li, 2007; Yui et al., 2012; Faure et al., 2016; Xu et al., 2017). A drastic transformation from active to passive margin followed during the late Mesozoic (Li et al., 2012). The northern SCS Basin basement was considered as the southward extension of the South China Block, where thinned continental crust displays variable thicknesses (Hayes and Nissen, 2005; Lei and Ren, 2016; Lei et al., 2019a). According to Sun et al. (2014), lower-to-upper Paleozoic strata are supposed to be unevenly preserved in the Beibu Gulf Basin, western Zhujiang River Mouth Basin and Taixinan Basin (Fig. 1a). In early studies, sedimentary facies and seismic lines indicated that the pre-Cenozoic basement was divided into several separate sections and displayed an eastward trending of younger ages (Wang et al., 2002; Sun et al., 2014). The case lacking geochronological evidence has been changed until recent detrital zircon U-Pb dating results were obtained. Therein, two granite dredge samples were dated with magmatic ages varying from 159 Ma to 127 Ma in Nansha area (Yan et al., 2010) (Fig. 1b). Additionally, Xisha area, to the southeast of Hainan Island, was previously postulated to be part of the Precambrian crystalline basement dated by Rb-Sr isochrones (Qin, 1987). Instead, the updated U-Pb age has confirmed its late Jurassic amphibole plagiogneisses which was later intruded by Cretaceous magmatic bodies (Zhu et al., 2017). Therefore, it is questionable whether the Paleozoic or even Precambrian strata have ever been widely distributed beneath the Cenozoic northern SCS sediments? In addition, located in the conjunction of Yinggehai Basin, Qiongdongnan Basin and Zhujiang River Mouth Basin, the Hainan Island together with other dispersed micro-blocks were rifted from Gondwana supercontinent during the opening of the Palaeo-Tethys in the Devonian (Metcalfe, 1996, 2011, 2013; Xu et al., 2008). Numerous researches show that the Hainan Island has recorded multiple thermal events and tectonic regime transitions since the late Paleozoic (Li et al., 2006; Jiang et al., 2015; Yao et

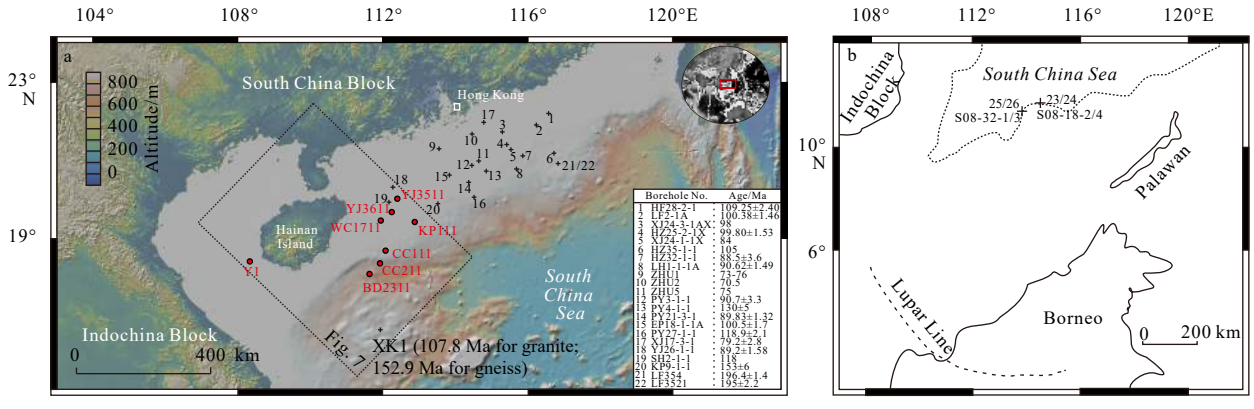

Fig. 1. Map of Beibu Gulf Basin, Yinggehai Basin, Qiongdongnan Basin and Zhujiang River Mouth Basin in the South China Sea with studied borehole samples and published data (a). Plot zoomed out in the upper right corner shows the study area under the global background. Red filled circles represent the analyzed boreholes of detrital zircon U-Pb dating or elemental geochemistry in this study. Black numbered crosses mainly centralized in the northeastern Zhujiang River Mouth Basin show some important samples analyzed by U-Pb, K-Ar or Rb-Sr dating in other studies. XK1 is from Zhu et al. (2017). Ages of these previous researches are shown in the lower right corner (Qiu et al., 1996; Li et al., 1999; Xu et al., 2017). For detailed sample information, refer to Tables 1 and 2. Sketch map of the Nansha area (b), its surrounding terranes and two dredge sampling locations (black cross) (Yan et al., 2010).

al., 2017). As a key component of the SCS region, the Hainan Island as well as its surrounding areas still require further basement evaluation.

Principle of isostatic balance and gravity-field modeling are helpful in estimating the lateral density or thickness variations of the interior structure of the lithosphere (Braitenberg et al., 2006; Ebbing et al., 2006; Franke et al., 2011). These are essential methods and techniques in revealing lithospheric velocity anomalies. Another technique involves magnetic anomaly interpretations, which could reflect directions and speeds of the ridge spreading processes (Briais et al., 1993; Hsu et al., 2004; Braitenberg et al., 2006; Li et al., 2008a, 2008b; Barckhausen et al., 2014). However, amplitudes of the basement features may be reduced in special cases where anomalies bend or two distinct directionalities meet. Moreover, due to the thick Cenozoic sedimentary blanket, the underlying flat-appearance structure might conceal different tectonic lineaments, tilted crustal highs, complicate-oriented ridges or faults. Therefore, ocean bottom topography not well charted could be very misleading in the crustal structure evaluation. Except for the weaknesses of the typical geophysical techniques, the subsequent rifting processes might also produce certain alteration onto the original pre-Cenozoic crustal structure (Nissen et al., 1995a, 1995b). In this case, the amount of crustal extension might be manifested in complicated manners in response to effective strengths, thicknesses, thermal structures and other rheological features according to disparate formation ages (Ebinger and Hayward, 1996; Clift and Lin, 2001; Qiu et al., 2001). For instance, the eastern SCS Basin basement generated widespread granite and sedimentary rocks during the late Mesozoic, where much extension is concentrated within younger, weaker and more ductile zones. Within the basement near eastern Hainan Island, on the other hand, the Paleozoic crust tends to be stretched in a similar degree to the more ancient Proterozoic crust (Hayes and Nissen, 2005). Hence, without constraints from any other supportive dating analyses, these geophysical parameters are likely to allow possible uncertainties.

Due to the limitation of the basinal geological evidence and ongoing controversy over the formation of the pre-Cenozoic basement, this study aims to present a comprehensive interpretation by deriving a dense set of data, including petrographic identification, elemental geochemistry analysis, gravity-magnetic joint inversion and zircon U-Pb dating. Specifically, zircons are considered as a kind of widely formed and extremely stable minerals, which are resistant to chemical alteration by long-distance sedimentation and low- or medium-degree metamorphism. Since U-Pb isotopic system possesses the highest closure temperature, it is optimal to use U-Pb dating for the age determination of igneous or high-grade metamorphic rocks. Lithological combination characteristics and gravity-magnetic constraints are also instrumental in examining whether the results are internally consistent in this study. Questions remaining to be answered include: (1) what is the precise aging framework for the pre-Cenozoic SCS Basin basement? (2) what types of rock assemblages have been generalized with respect to different sections of the SCS Basin basement? (3) what tectonic events and geodynamic processes might have caused such distribution patterns of the answers to questions 1 and 2?

2 Geological history

The southeastern Asia was principally under control from two of the most critical geodynamic domains: the Paleo-Pacific subduction zone to the east and the Tethys subduction zone to the west (Carter et al., 2001; Li and Powell, 2001; Hall, 2002, 2012; Lepvrier et al., 2004; Zhou et al., 2008; Wallace et al., 2009; Li et al., 2011). A general consensus is reached that a well-developed Andean-type of volcanic arc existed along the southeastern Asian margin (e.g. South China southeastern margin) lasting from Triassic-Jurassic to Cretaceous (Maruyama, 1997; Zhou and Li, 2000; Li and Li, 2007; Li et al., 2012). The Paleo-Pacific subduction beneath the eastern Asian margin led to extremely drastic and complex tectonic activities across the South China Block. Multi-stage structural deformation, magmatism as well as local stress field changes took place in this region (Jahn et al., 1990; Zhou et al., 2006; Li et al., 2014). Further west, the Indochina Block collided obliquely with the South China along the Song-Ma Suture and Red River Fault Zone (Leloup et al., 2001; Lepvrier et al., 2004; Metcalfe, 2011, 2013). Therein, narrowing and closure of the Meso-Tethys was likely responsible for the late Triassic regional folding, uplifting and orogeny over the Indochina Continent (Metcalfe, 1996; Roger et al., 2000; Lepvrier et al., 2008; Sone and Metcalfe, 2008). Subsequently, the convergent Andean-type continental margin was transferred into the divergent western Pacific margin prior to the opening of the SCS (Zhou et al., 2006; Schellart et al., 2006; Li et al., 2012, 2014; Shi and Li, 2012). This sudden "transpression-transtension" switching process might be largely triggered by oceanward retreat of the Paleo-Pacific subduction zone in the late Mesozoic (Jahn et al., 1990; Lapierre et al., 1997; Li et al., 2014). The plate driving forces experienced fundamental changes during this time. Large-scale rifting started around the coastal South China, which resulted in the thinning of continental margin (Lei et al., 2019a). During the Eocene–early Miocene, southward slab pull of the oceanic crust led to elimination of the Proto-SCS (Hall, 2002, 2012; Morley, 2002; Hayes and Nissen, 2005). The present SCS was eventually generated, displaying a sequential pattern of continental margin–transitional crust–oceanic crust. During the long-term extensional and thermal-subsidence stages, thick sedimentary strata were formed over the SCS Basin basement during Cenozoic, and were influenced from different source-to-sink systems (Shao et al., 2015, 2017, 2019; Cao et al., 2018; Lei et al., 2018, 2019b). These sedimentary basins mainly include the Beibu Gulf, Yinggehai, Qiongdongnan and the Zhujiang River Mouth Basin (Briais et al., 1993; Rangin et al., 1995; Yao, 1996; Morley, 2002, 2016) (Fig. 1a).

Previous studies show that a number of East Asian and Southeast Asian continental terranes, e.g. the North China Block and the South China Block, the Indochina Block, have the origin of the northern Gondwana supercontinental margin (Veevers, 2004; Metcalfe, 2011; Cocks and Torsvik, 2013; Metcalfe, 2013). Separation, drifting and amalgamation of the Gondwana-related continental blocks as well as the accompanying oceans might have largely shaped the southeastern Eurasian margin before Cenozoic (Metcalfe, 1996). As a key region of the southeast Asia, the SCS Basin basement has been the focus of numerous plate geodynamic reconstructions (Zhou et al., 2008; Metcalfe, 2011; Morley, 2012; Zhu et al., 2017). However, there are still hot debates on its tectonic affiliation. Some researchers propose that the pre-Cenozoic lithospheric layer was partly derived from the South China terrain, i.e., discrete micro-fragments of the Beibu Gulf Basin together with the Hainan Island. These micro-terranes were inferred to commonly develop on a Proterozoic folded continental massif (Liu et al., 2006, 2011; Li et al., 2008c; Sun et al., 2014). Other scholars suggest that the SCS Basin basement is likely to be a missing linkage (or an individual tectonic domain) between the Cathaysia Block and Indochina Block, which was dated by scattered Precambrian ages (Lan et al., 2003; Wan et al., 2006; Lu et al., 2011; Yu et al., 2012). To be noted, the early Paleozoic

metamorphism and magmatism have been confirmed within the Cathaysia Block and Indochina Block by massive geochronological and thermochronological studies (Lepvrier et al., 2008; Charvet et al., 2010; Wang et al., 2011; Vượng et al., 2013; Faure et al., 2014). Therefore, it also suggested that the SCS Basin basement dominated by Paleozoic strata, i.e., Yinggehai Basin, the east of Hainan Island, etc. was mainly sourced from the Paleozoic outer extension of the Cathaysia Block or Indochina Block. Previous studies mainly concentrated on the Zhujiang River Mouth Basin of the northeastern SCS were also reanalyzed (Qiu et al., 1996; Li et al., 1999; Xu et al., 2017). As complementary information, the data synthesis will largely enable us to obtain a more comprehensive interpretation across the whole basement (refer to Fig. 1 and Table 1 for geographical locations and more details of the published data).

3 Analytical procedures

In order to verify the complicated nature of the basement structure and its regional tectonic significance, this study collected one biotite granite and eight metamorphic clastic rock samples for geochemistry and geochronology analysis together with petrography identification (refer to Table 2 for detailed sample information on detrital zircon U-Pb geochronology study). These samples were straight drilled through the pre-Cenozoic basement by the China National Offshore Oil Corporation.

3.1 *Elemental geochemistry analysis*

Geochemical analyses for the SCS Basin basement metamorphic clastic rock samples were carried out at the State Key Laboratory of Marine Geology of Tongji University, China. After being washed by deionized distilled water, bulk sediments were then dried at 50°C for 48 h to prevent external contamination. Meta-sedimentary rocks were heated to 600°C for 2 h to remove the organic matter and interlayer water. Dissolved in a 1:1 HF-HNO_3 mixture, samples were finally measured for their major and trace elemental concentration. The instrumentation was constituted by an inductively coupled plasma optical emission spectrometry (ICP-OES, Thermo Fisher Scientific, USA) and Thermo Elemental X-Series inductively coupled plasma mass spectrometry (ICP-MS, Thermo Fisher Scientific, USA), respectively. Three certified materials (GSR-5, GSR-6, and GSD-9 from the Institute of Geophysical and Geochemical Exploration, China) were repeatedly used as unknown samples for the precision and accuracy assessment. The external precision (1 σ) was generally better than 5% for trace elements (Fig. 2). And results were usually in agreement with the reference materials (modified from Li et al. (2003) and Wei et al. (2006)).

3.2 *Detrital zircon U-Pb dating*

In this study, zircon grains were separated from meta-sedimentary rocks using standard density and magnetic separation techniques at the laboratory of the Institute of Regional Geology and Mineral Resources, Hebei, China. Over 200 chosen zircons were randomly pasted on adhesive tape and then cast in an epoxy mount prior to the polishing process. Zircons were examined with cathodoluminescence images (CL) to determine their internal structures and microzonation positions (20–30 μm) (refer to Fig. 3 for CL images of representative samples). Meas-

Table 1. Summary of published data of SCS pre-Cenozoic basement (refer to Fig. 1 for detailed sample locations)

Number in Fig. 1a	Sample No.	Depth/m	Isotopic ages/Ma	Analytical method	Lithology	References
1	HF28-2-1	3 942.0–3 943.6	109.25±2.40	K-Ar	cataclastic granodiorite	Li et al. (1999)
2	LF2-1A	2 480.0–2 483.5	100.38±1.46	K-Ar	cataclastic dimicaceous granite	Li et al. (1999)
2	LF2-1A	2 480.0–2 483.5	94.83±1.89	Rb-Sr	cataclastic dimicaceous granite	Li et al. (1999)
3	XJ24-3-1AX	4 318–4 319	98	K-Ar	cataclastic granite	Li et al. (1999)
4	HZ25-2-1X	3 196.4	99.80±1.53	K-Ar	cataclastic granite	Qiu et al. (1996)
5	XJ24-1-1X	3 851.0–3 851.5	84	K-Ar	granite	Li et al. (1999)
6	HZ35-1-1	2 218.9	105	K-Ar	cataclastic quartz diorite	Li et al. (1999)
7	HZ32-1-1	2 791	88.5±3.6	K-Ar	cataclasitc granite	Li et al. (1999)
8	LH1-1-1A	1 836.5	90.62±1.49	K-Ar	cataclastic granodiorite	Li et al. (1999)
8	LH1-1-1A	1 822.0–1 837.5	72.78±1.37	Rb-Sr	cataclastic granodiorite	Li et al. (1999)
9	ZHU1	1 846–1 847	73–76	K-Ar	granite	Li et al. (1999)
10	ZHU2	2 379–2 380	70.5	K-Ar	biotite granite	Li et al. (1999)
11	ZHU5	3 261.8–3 262.3	75	K-Ar	granite porphyry	Li et al. (1999)
12	PY3-1-1	3 192	90.7±3.3	K-Ar	granite	Li et al. (1999)
13	PY4-1-1	3 160	130±5	K-Ar	granite	Qiu et al. (1996)
14	PY21-3-1	4 068.0–4 019.5	89.83±1.32	K-Ar	cataclastic biotite granite	Li et al. (1999)
15	EP18-1-1A	3 448.25	100.5±1.7	K-Ar	granite	Qiu et al. (1996)
16	PY27-1-1	3 607–3 609	118.9±2.1	K-Ar	quartz monzonite	Li et al. (1999)
17	XJ17-3-1	2 122–2 124	79.2±2.8	K-Ar	cataclastic granite	Li et al. (1999)
18	YJ26-1-1	1 700–1 702	89.20±1.58	K-Ar	rhylote porphyry	Li et al. (1999)
19	SH2-1-1	3 641.2	118	K-Ar	biotite hornblende diorite	Li et al. (1999)
20	KP9-1-1	1 662–1 774	153±6	K-Ar	cataclastic granite	Li et al. (1999)
21	LF354	2 472.3	196.4±1.4	U-Pb	granite	Xu et al. (2017)
22	LF3521	2 443.5	195.0±2.2	U-Pb	diorite	Xu et al. (2017)
23	S08-18-2	2 700	159.1±1.6	U-Pb	tonalite	Yan et al. (2010)
24	S08-18-4	2 700	157.8±1.0	U-Pb	tonalite	Yan et al. (2010)
25	S08-32-1	3 100	153.6±0.3	U-Pb	monzogranite	Yan et al. (2010)
26	S08-32-3	3 100	127.2±0.2	U-Pb	monzogranite	Yan et al. (2010)

Table 2. List of samples analyzed for Laser-ICP-MS detrital zircon U-Pb dating (refer to Fig. 1a for detailed sample locations)

Borehole No.	Geographical location	Sampling depth/m	Depth of basement/m	Previous geological times	Youngest age/Ma	Oldest depositional ages	Lithology
Y1	Yinggehai Basin	3 021–3 023	3 021	?	1 264±83	Precambrian	metamorphic biotite granite
WC1711	Qiongdongnan Basin	2 216	2 216	Paleozoic	114±4	early Cretaceous	meta-tuff
CC211	Qiongdongnan Basin	1 116	1 076	Paleozoic	129±7	early Cretaceous	meta-tuff
KP111	Zhujiang River Mouth Basin	1 893–1 897	1 884	Paleozoic	124±3	early Cretaceous	volcaniclastic rock
BD2311	Qiongdongnan Basin	2 166	2 166	Paleozoic	85±3	late Cretaceous	metamorphic quartzose sandstone
CC111	Qiongdongnan Basin	1 172	1 117	Paleozoic	125±4	late Cretaceous	metamorphic sandstone
YJ3511	Zhujiang River Mouth Basin	4 321–4 339	4 321	Paleozoic	88±2	late Cretaceous	metamorphic siltstone
YJ3611	Zhujiang River Mouth Basin	3 565–3 580	3 484	Paleozoic	88±2	late Cretaceous	metamorphic mudstone and siltstone

Note: ? represents not have been dated before.

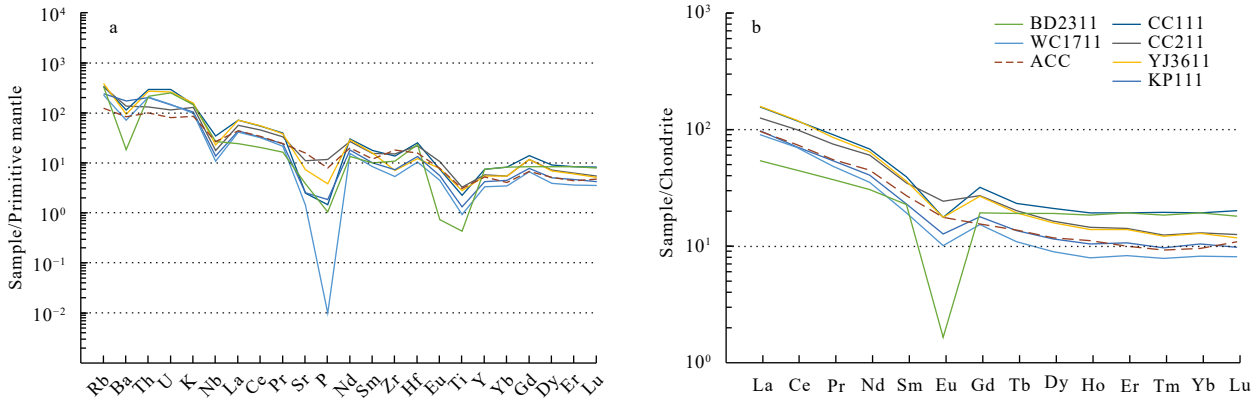

Fig. 2. Primitive mantle-normalized trace element spider diagrams (a) and chondrite-normalized rare earth elements (REE) distribution patterns (b) for the SCS Basin basement samples. Trace elements of the primitive mantle and chondrite REE are from Sun and McDonough (1989) and Taylor and McLennan (1985), respectively. Average continental crust (ACC) are from Rudnick and Gao (2003).

urements of U, Th and Pb were later conducted at the State Key Laboratory of Marine Geology of Tongji University, China. The instrumentation is composed of a Thermo Elemental X-Series ICP-MS coupled to a New Wave 213 nm laser ablation system (Shao et al., 2016). Typically, 5-scan cycles were conducted for each analysis with a spot diameter of 30 μm. The 91 500 external standards ((1 065.4±0.3) Ma) were interspersed with tested samples to calculate isotopic ratios by ICPMSDataCal (Wiedenbeck et al., 1995; Liu et al., 2010). The glass NIST 610 was used to optimize the machine as an internal standard. Accuracy of our analytical results was validated by reference material Plešovice with an age of (337.1±0.4) Ma (Sláma et al., 2008). Measured compositions have been corrected for common Pb using the method of Andersen (2002). The $^{206}Pb/^{238}U$ and $^{207}Pb/^{206}Pb$ ages were finally adopted for younger or older zircons of 1 000 Ma, respectively. Wherein, uncertainties on individual U-Pb analyses are quoted at the 1 σ level. Age distributions in this study and other published documents are visualized as histograms and kernel density estimation plots (Vermeesch, 2012).

3.3 *Gravity-magnetic-seismic joint inversion*

Both gravimetric and magnetic measurements have been conducted in the study area. Free-air gravity anomalies were originally extracted from satellite-derived data of 2-min grid (Sandwell and Smith, 1997). Since there is an obvious density contrast around the Cenozoic-Mesozoic regional unconformity, free-air gravity anomalies are sensitive to undulations caused by rifting and faulting structures in the pre-Cenozoic basement. The total field magnetic anomalies also contain rich geological implications. However, they could possibly be biased at middle-to-low latitudes because of the oblique inclinations of induced magnetizations. To facilitate the precision of our data interpretation, this study processed the magnetic anomalies calculation (source from compilation by Geological Survey of Japan and Coordinating Committee for Coastal and Offshore Geoscience Programmes in East and Southeast Asia (CCOP), 1996) by reducing to the pole (RTP magnetic anomalies), which are sharper to the existence of magmatic bodies. Here this study has also compiled seismic profiles and reconstructed the major stratigraphic framework to generalize a set of models between travel time and depth. In addition, this study obtained the relationship between travel time and rock density by conducting an integrated investigation on different types of rocks over the northern SCS Basin basement. This gravity-magnetic-seismic joint inversion shows less uncertainties and artificialities, which is largely discriminative from both traditional stripping method and interactive interpretation model. By recognizing the existence of geological anomaly bodies, this study is able to better describe the pre-Cenozoic SCS Basin basement.

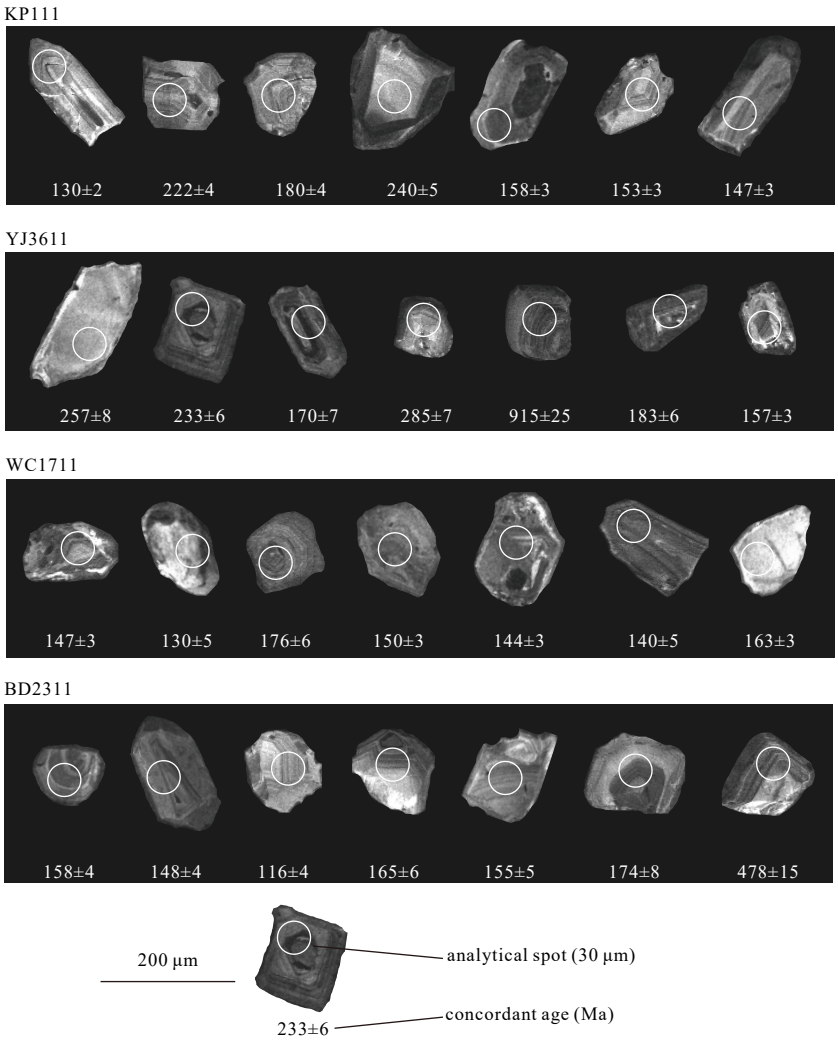

Fig. 3. Representative cathodoluminescence images showing the internal structures of the zircon grains and associated U-Pb ages.

4 Results

4.1 *Geochemical variations*

Primitive mantle-normalized trace element and chondrite-normalized rare earth element (REE) spider diagrams for the basement samples are exhibited in Fig. 2. Overall, the trace element distribution patterns are reported to be modestly different from the average continental crust (Rudnick and Gao, 2003). In the primitive mantle-normalized trace element diagram (Fig. 2a), our samples show obvious negative anomalies in element Ba, Nb, P and Ti while weak enrichment in element Rb, Th, U and K (regarded as heat-producing or radioactive elements). Chondrite-normalized REE patterns, on the hand, commonly display steep slopes with distinct negative Eu anomalies. Enrichment of light REE (LREE) ($(La/Yb)_N$=0.65–59.46) can be seen with an assemblage of pronounced Eu depletions (Eu/Eu*=0.03–0.98, with a few exceptional analyses of 1.08, 1.44 and 1.92) (Fig. 2b). One single analysis of $(La/Yb)_N$ is lower than 1 (0.65) for borehole BD2311. Slightly distinct from the other boreholes, BD2311 is characterized by a relatively flat pattern with an extremely negative Eu anomaly averaging at 0.09.

4.2 *U-Pb geochronology*

As observed in CL images of representative samples (Fig. 3), the clear oscillatory zones obviously indicate their magmatic origin for the analyzed zircon grains (Hoskin and Schaltegger, 2003). In addition, most Th/U ratios from the SCS Basin basement samples range between 0.1 and 1 (Fig. 4). U-Pb Concordia diagrams are shown in Fig. 5. Figure 6 shows the histograms and probability density distribution patterns, which are grouped respectively according to their peak combinations. Results of the detrital zircon U-Pb dating are outlined as follows according to lithological descriptions and their individual spectra features.

To the east of Hainan Island, the meta-tuff sample WC1711 is featured by rounded, sub-rounded to euhedral zircon grains with oscillatory zonings (Fig. 1a). WC1711 has a modestly wide variation of Th (110.26×10^{-6}–$3\,501.78\times10^{-6}$) and U (152.23×10^{-6}–$3\,729.32\times10^{-6}$) content, producing Th/U ratios larger than 0.1 (Fig. 4). Of all the sixty-five effective analyses, the youngest U-Pb age is (114±4) Ma. Apart from one inherited $^{207}Pb/^{206}Pb$ age of (2 503±42) Ma, WC1711 gives a major population of $^{206}Pb/^{238}U$ ratios between (114±4) Ma and (252±6) Ma, forming an upper Jurassic cluster centralized at ca. 150 Ma (Fig. 6a). Another meta-tuff sample CC211 is located further south to sample WC1711. Th and U contents are 86.29×10^{-6}–$1\,756.57\times10^{-6}$ and 150.73×10^{-6}–$3\,482.09\times10^{-6}$, respectively. Th/U ratios range between 0.34 and 1.14. Of all the sixty-four analyses, the youngest U-Pb age is (129±7) Ma. Aside from one single Paleozoic analysis ((342±10) Ma), the re-

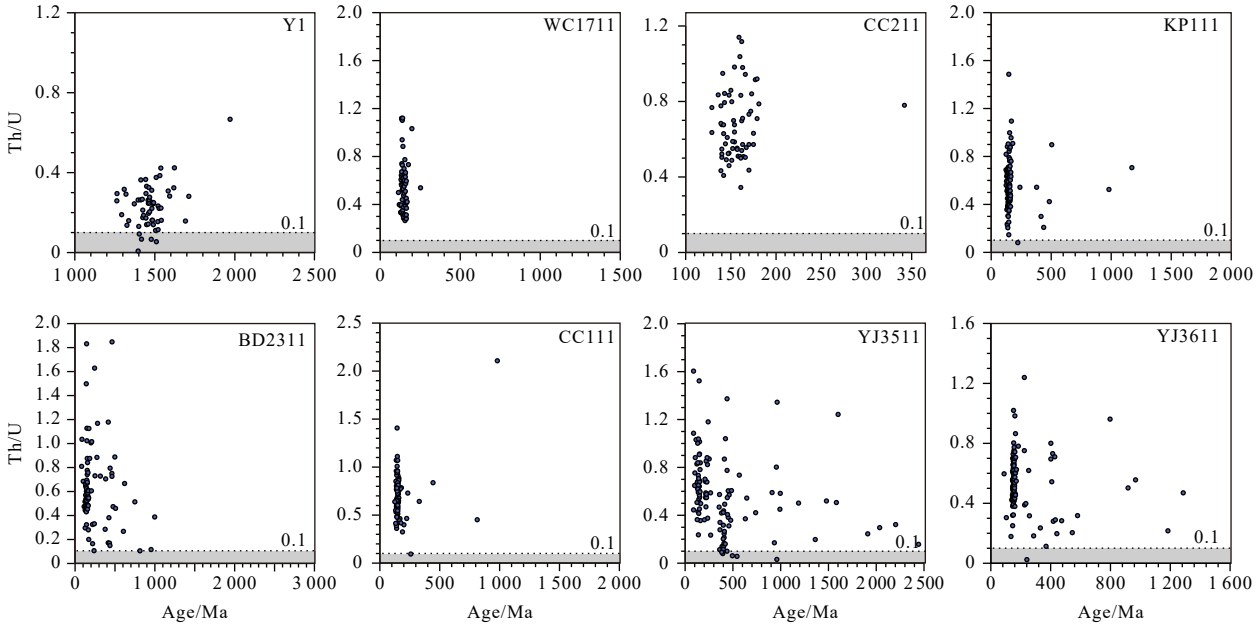

Fig. 4. Summary of the Th/U ratios versus U-Pb ages of the studied zircon grains from the SCS Basin basement. Grey shades indicate the Th/U variations are lower than 0.1.

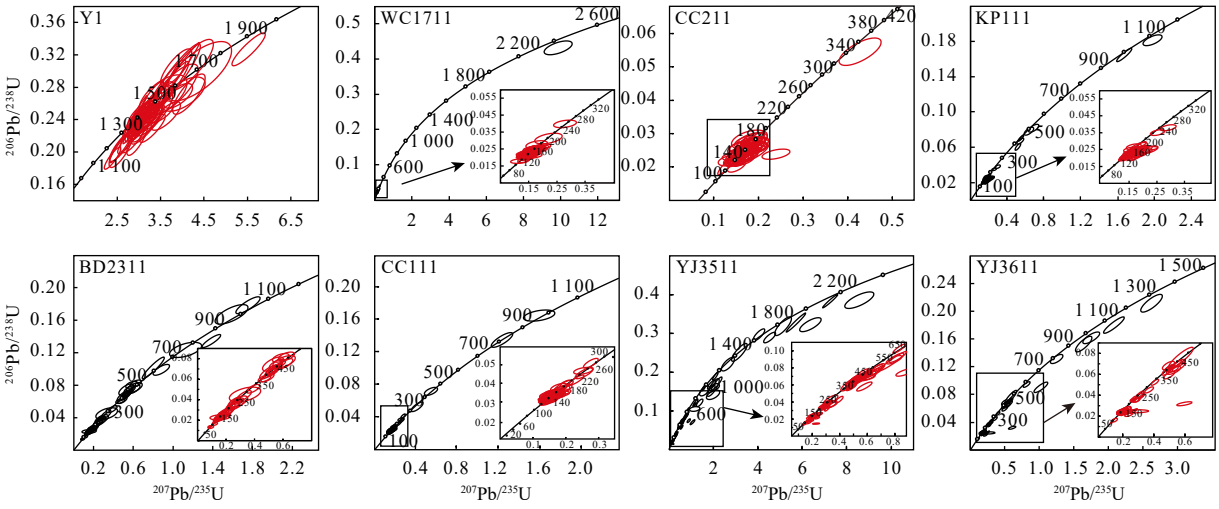

Fig. 5. Detrital zircon U-Pb Concordia diagrams for the SCS Basin basement samples. The lower right corner plots in some diagrams show magnified Concordia ages for samples WC1711, CC211, KP111, BD2311, CC111, YJ3511 and YJ3611. The numbers on the curve represent concordia U-Pb ages of a standard zircon grain.

maining are centralized at ca. 150 Ma.

Metamorphic sandstone CC111 is mostly characterized by sub-euhedral and euhedral zircon grains (Fig. 1a). Of all the ninety analyzed spots, Th (111.24×10^{-6}–1 897.93×10^{-6}) and U (202.82×10^{-6}–4 722.91×10^{-6}) concentrations are modestly high and variable. Almost all the analyses have Th/U ratios exceeding 0.1. About 94% of total spots are Mesozoic ages, based on $^{206}Pb/^{238}U$ ratios from (125±4) Ma to (233±5) Ma (Fig. 6a). The other five analyses include three Paleozoic ages (258±6) Ma, (329±14) Ma, (444±12) Ma), and two Proterozoic ages ((813±21) Ma, (981±15) Ma).

Volcaniclastic rock KP111 is dominated by euhedral to sub-euhedral grains with clear internal core-rim structures (Fig. 1a). Of the 117 analyzed spots, Th and U concentration is characterized by a broad variation from 32.24×10^{-6} to 2 730.38×10^{-6}, and from 95.13×10^{-6} to 4 055.87×10^{-6}, respectively. KP111 has only one single Th/U analysis of 0.08 (Fig. 4). Two Proterozoic spots with ages of (982±17) Ma and (1 173±31) Ma probably indicate inherited cores. There are108 concordant ages mostly fall within the group of Mesozoic 240–124 Ma (centralized around 145 Ma). Scattered spots are of Paleozoic 505–379 Ma ages. The youngest age of sample KP111 is (124±3) Ma (Fig. 6a).

Sample YJ3511 is extracted from a metamorphic siltstone. A total of 126 analyses were conducted on this sample. Th and U contents highly varied between 136.84×10^{-6} and 7 900.79×10^{-6}, between 110.07×10^{-6} and 10 989.99×10^{-6}, respectively. Six analyses display Th/U ratios falling between 0.03 and 0.10 (Fig. 4). The other analyses range between 0.11 and 1.60. YJ3511 shows an apparent peak at ca. 135 Ma and a subordinate peak at ca. 405 Ma (Fig. 6b). In detail, thirty-eight Paleozoic ages range between

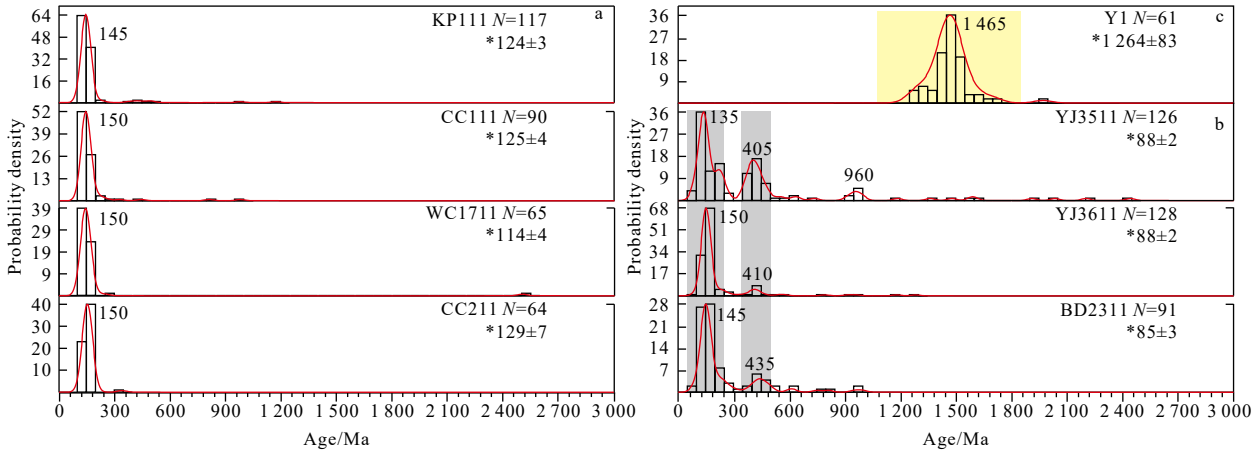

Fig. 6. Histograms and probability density distribution plots for detrital zircon U-Pb ages of the SCS Basin basement samples with characteristic age peaks numbered. Age spectra are grouped according to their specific distribution patterns into (a)–(c) sub-plots. *N* represents the number of concordant analyses for each sample. The youngest zircon U-Pb age in red is marked with * in the upper right corner. Dominant age peaks of sample Y1 are highlighted in light yellow shades; major peaks of YJ3511, YJ3611 and BD2311 are in gray shades.

(252±5) Ma and (495±10) Ma, while twenty-one Proterozoic ages range between (543±27) Ma and (2 443±36) Ma. The metamorphic mudstone-siltstone sample YJ3611 is located close to YJ3511 (Fig. 1a). Of all the adopted ninety-one analyses, significantly high values are identified within Th (122.90×10^{-6}–$8\,349.25\times10^{-6}$) and U (373.64×10^{-6}–$33\,224.03\times10^{-6}$) concentrations. In addition to one analysis at 0.02, the other spots have Th/U ratios falling between 0.11 and 1.24 (Fig. 4). About 90% of the total concordant $^{206}Pb/^{238}U$ values yield a large Mesozoic cluster at ca. 150 Ma. The rest, on the other hand, range between (252±5) Ma and (1 283±47) Ma (twenty-one analyses in total). Comparatively, the Caledonian peak at ca. 410 Ma is not as obvious as YJ3511. Both samples YJ3511 and YJ3611 have the youngest age of (88±2) Ma (Fig. 6b).

Sample BD2311 is from a metamorphic quartzose sandstone rock, located to the southeast of Hainan Island (Fig. 1a). It has modestly variable Th (37.62×10^{-6}–$6\,348.54\times10^{-6}$) and U (72.99×10^{-6}–$4\,127.31\times10^{-6}$) concentrations. All Th/U ratios fall between 0.10 and 1.85 (Fig. 4). More than 80% of the total calculations are centralized as a dominant Mesozoic age at ca. 145 Ma. Similar to sample YJ3611, the Caledonian cluster at ca. 435 Ma is not apparent on the U-Pb spectra of BD2311. The remaining twenty-six analyses in BD2311 include eighteen Paleozoic (509–252 Ma) and six Proterozoic zircons (998–607 Ma). Of all the 91 effective analyses, the youngest age of sample BD2311 is (85±3) Ma (Fig. 6b).

Sample Y1 is a metamorphic biotite granite to the west of Hainan Island (Fig. 1a). Its rounded to sub-rounded zircon crystals retain magmatic growth zonation, which commonly have light-color melting rims, range from 50 μm to 100 μm in length, and are featured by length to width ratios of ca. 1:1 to 2:1. Th concentration is modestly lower (25.09×10^{-6}–371.50×10^{-6}) while U concentration is higher and more variable (191.30×10^{-6}–$3\,362.47\times10^{-6}$), producing Th/U ratios with relatively lower values ranging between 0.01 and 0.40 (only a single Th/U analysis of 0.67).

Five analyses display Th/U ratios falling between 0.01 and 0.10. Much distinctive from other samples of younger depositional ages, Y1 shows an apparent Proterozoic cluster of concordant $^{207}Pb/^{206}Pb$ ratios from (1 264±83) Ma to (1 714±52) Ma in addition to an age of (1 972±23) Ma. These data commonly form a predominant Meso-Proterozoic population clustering at ca. 1 465 Ma (Fig. 6c).

4.3 *Lithological and petrographical identification*

Mineral composition, content, structure and texture were identified and classified for each sample under both crossed and polarized light microscope. Figure 7 shows the representative rock samples of KP111, YJ3511, YJ3611 and Y1. The volcaniclastic rock sample KP111 is comprised of metamorphic pyroclastic and quartzite (Figs 7a and b). Obvious porphyritic structures were generated in sample KP111, of which phenocrysts are mainly quartz grains. The corrosion structures and micro-surface cracking of the minerals imply the drastic temperature changes during eruptions. The matrix minerals are mainly comprised of microcrystalline feldspar and quartz which were formed during vitric recrystallization. KP111 also displays obvious high sericite contents and slight-to-moderate directional alignments. Similarly, the mosaic structures and directional arrangements are also identified within the quartzite composition. Sample YJ3511 is comprised of low-degree slates and metamorphic siltstones (Figs 7c and d). The slates are mainly composed of cryptocrystalline or microcrystalline clay minerals. The metamorphic siltstones, on the other hand, are mostly microcrystalline quartz and feldspar minerals with some directionally arranged schistose minerals, e.g. metamorphosed sericite. Sample YJ3611 mainly consists of low-degree metamorphic mudstones and siltstones (Figs 7e and f). The metamorphic mudstones contain cryptocrystalline clay minerals, in addition to low contents of quartz and microcrystalline feldspar. The metamorphic siltstones, on the other hand, contain microcrystalline quartz and feldspar, which commonly display mosaic textures and directional alignments. The westernmost sample Y1 is featured by an obvious granitic texture, including orthoclase, quartz and low contents of plagioclase and biotite (Figs 7g and h). Kaolinization, carbonatization and sodium zoisitization are identified within feldspar, while chloritization is observed within biotite.

5 Discussion

5.1 *Petrogenesis based on elemental geochemistry and petrography studies*

Samples KP111, YJ3511 and YJ3611 are typically low-degree metamorphic rocks. They commonly display high content of metamorphosed sericite, mosaic structures and slight-to-moder-

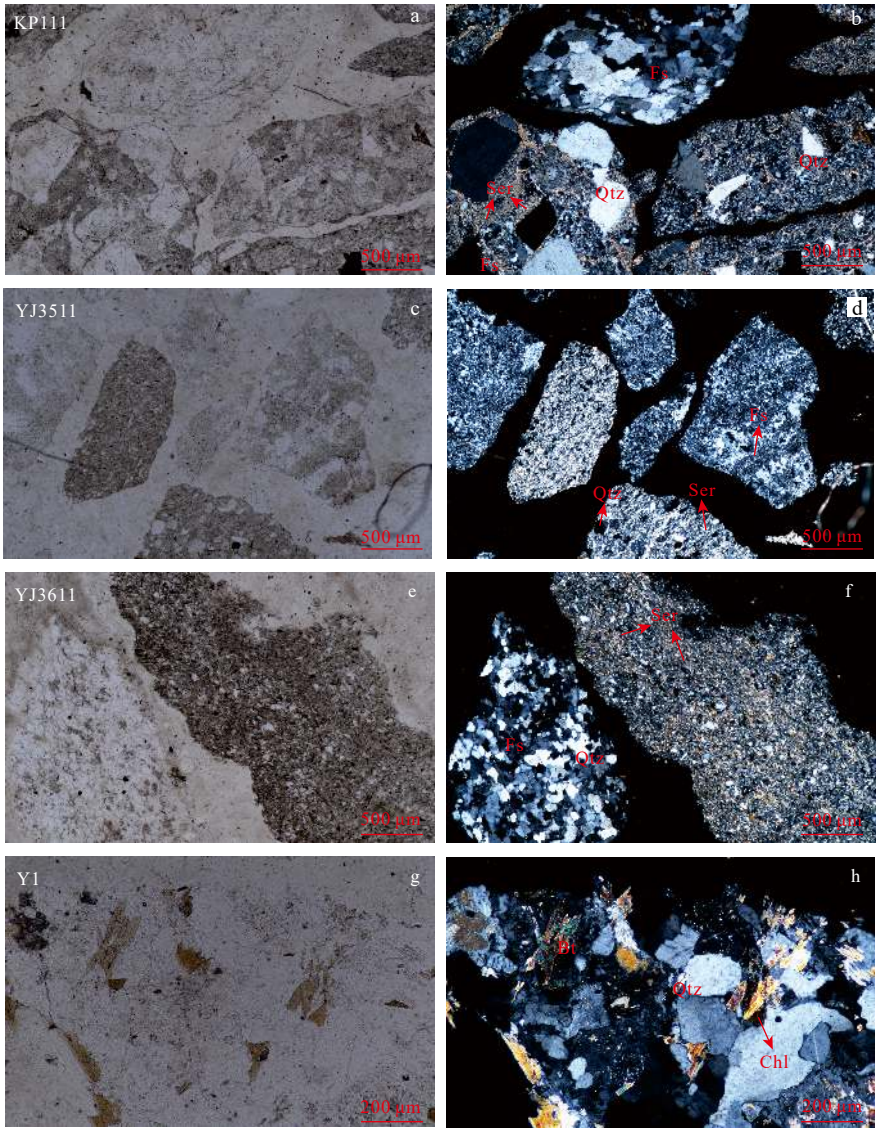

Fig. 7. Lithological and petrographic characteristics of SCS Basin basement samples under both plane-polarized light and cross-polarized light microscope. a. KP111, metamorphic volcaniclastic rock; c. YJ3511, metamorphic siltstone; e. YJ3611, metamorphic mudstone and siltstone; g. Y1, metamorphic biotite granite slices under plane-polarized light; b. KP111, d. YJ3511, f. YJ3611 and h. Y1 slices under cross-polarized light. Fs: feldspar, Qtz: quartz, Ser: sericite, Bt: biotite, Chl: chlorite. Refer to Fig. 1 for detailed sample location.

ate directional alignments (Figs 7a–f). KP111 is also marked by clear melting-corrosion textures and fission cracks on its quartz phenocrysts. The other meta-sedimentary samples, YJ3511 and YJ3611, are observed with palimpsest structures (or relict structures) within their meta-mudstone or siltstone components, which indicate incomplete recrystallization processes and preservation of the original mineral textures. To the west of Hainan Island, sample Y1 is uniquely featured by muscovite alteration and might have experienced metamorphism by displaying more evident directional arrangements of chlorite, muscovite and quartz minerals (Figs 7g and h). However, zircon grains of metamorphic origin were actually not generalized in this study since the samples are mostly featured by Th/U values exceeding 0.1 (Fig. 4).

High field strength elements (HFSE) are typically regarded as relatively immobile elements which are least susceptible to metamorphism and alteration, such as Nb, Ta, Zr, Hf, Th, etc. The studied samples exhibit Ba, Nb, Ti and P negative anomalies, weak-to-strong positive anomalies in Rb, K, Hf and several heat-producing or radioactive elements Th and U (Fig. 2a). To be noted, concurrent existences of Nb-Ti depletion and Rb enrichment could not be simply attributed to fractional crystallization. According to Pearce (1983), the large ion lithophile elements (LILE) abundances and HFSE depletion are indicative of the arc affinity and source characteristics. As implied by previous researches, Hf enrichment or Nb-Ti depletion in arc-related rocks can be explained by slab-derived melts or subducted sediments (Pearce and Peate, 1995). In this study, positive anomalies of fluid-mobile element Rb together with melt-mobile elements Th and LREE commonly indicate fluid and melting in the SCS Basin basement rocks. Consistently, REE patterns in the samples are almost entirely featured by considerably negative Eu anomalies (Eu/Eu* values vary from 0.03 to 0.98), and LREE enrichment with broadly variable $(La/Yb)_N$ ratios from 0.65 to 59.46 (Fig. 2b).

As a preliminary conclusion, geochemical results and petrographic thin sections commonly indicate that source magma rocks might have been metasomatized by subduction-released fluids and hydrous melting materials.

5.2 *Geochronology and texture reinterpretation of the northern SCS Basin basement*

It was previously postulated that the pre-Cenozoic SCS Basin residual basement was divided into several parts by near N-S or NW–SE directional faulting and rifting (Wang et al., 2002; Liu et al., 2006, 2011; Lu et al., 2011; Sun et al., 2014). Unfortunately, most of these basinal areas were roughly constrained by petrographic observation and deep seismic reflections, which lacked high-precision dating analyses (Dien et al., 1998; Nielsen et al., 1999; Wan et al., 2006; Hao et al., 2011; Sun et al. 2014). The poor geochronological investigation has long been a hindrance for the SCS Basin basement interpretation. However, Zhu et al. (2017) recently revealed the Xisha late Jurassic ((152.9±1.7) Ma) to early Cretaceous (137 Ma) metamorphism as well as the Cretaceous ((107.8±3.6) Ma) granite intrusive ages. These updated dating studies are contrast with the antecedent Rb–Sr isochron age of 627 Ma (Qin, 1987). The fairly young U-Pb ages cast further doubts on the traditional understanding of the wide distribution of ancient Precambrian or Paleozoic basement.

According to our kernel density estimate plotting, most of the basement samples commonly display a prominent late Mesozoic cluster (Fig. 6a). The southernmost granite intrusion, represented by borehole XK1, is practically dated by a Cretaceous age of (107.8±3.6) Ma (Zhu et al., 2017). This sample provides reliable basinal evidence for the late Yanshanian magmatic activity surrounding the South China continental margin. To the east of Hainan Island, meta-clastic rocks have been first examined for U-Pb geochronology studies. The youngest U-Pb ages are generally considered as the largest deposition age. In view of the thick overlying Cenozoic successions, the studied zircon U-Pb ratios imply the formation of the extensive late Mesozoic strata (Fig. 8). Meta-tuffs and other meta-clastic samples, including KP111, CC111, WC1711 and CC211, commonly feature early Yanshanian ages (ca. 150–140 Ma) as their centralized age populations.

The remaining meta-sedimentary rock samples BD2311, YJ3511 and YJ3611 exhibit appearance of Caledonian peaks in addition to the dominant Yanshanian peaks (Fig. 6b). Briefly, the significantly high Yanshanian (ca. 150–135 Ma) and minor Caledonian (ca. 435–405 Ma) peaks could have been caused by provenance containing both Paleozoic and Mesozoic zircons. These sediments along with a small number of recycling Proterozoic grains were delivered into the areas to the east of Hainan Island. Based on petrographic identification and Th/U measurements, the studied meta-clastic samples mostly indicate low degree metamorphism. It is traditionally far below the thermal condition where zircon grains of metamorphic origin can be formed. Therefore, possibility could be excluded of certain that the younger peaks were caused by post-metamorphism in these bimodal-pattern U-Pb spectra. In other words, a population of metamorphosed zircon grains was unlikely to be subsequently generated from Mesozoic metamorphism, aside from their initial magmatic origin within source areas. These boreholes are also altogether characterized by youngest zircon ages of the late Cretaceous (Figs 6b and 8). Given the superimposed angular disconformity as a boundary between Cenozoic and pre-Cenozoic records, erosion and uplifting gradually ceased which were followed by a suite of sedimentary depositions in the western SCS region.

Additionally, the studied gravity-magnetic-seismic anomaly interpretations provide supporting evidence for a uniform Mesozoic SCS Basin basement (Fig. 9). The overall basement is more likely to generate relatively small-scale N-S directional faulting or rifting than previously being suggested (Fig. 9f, modified from

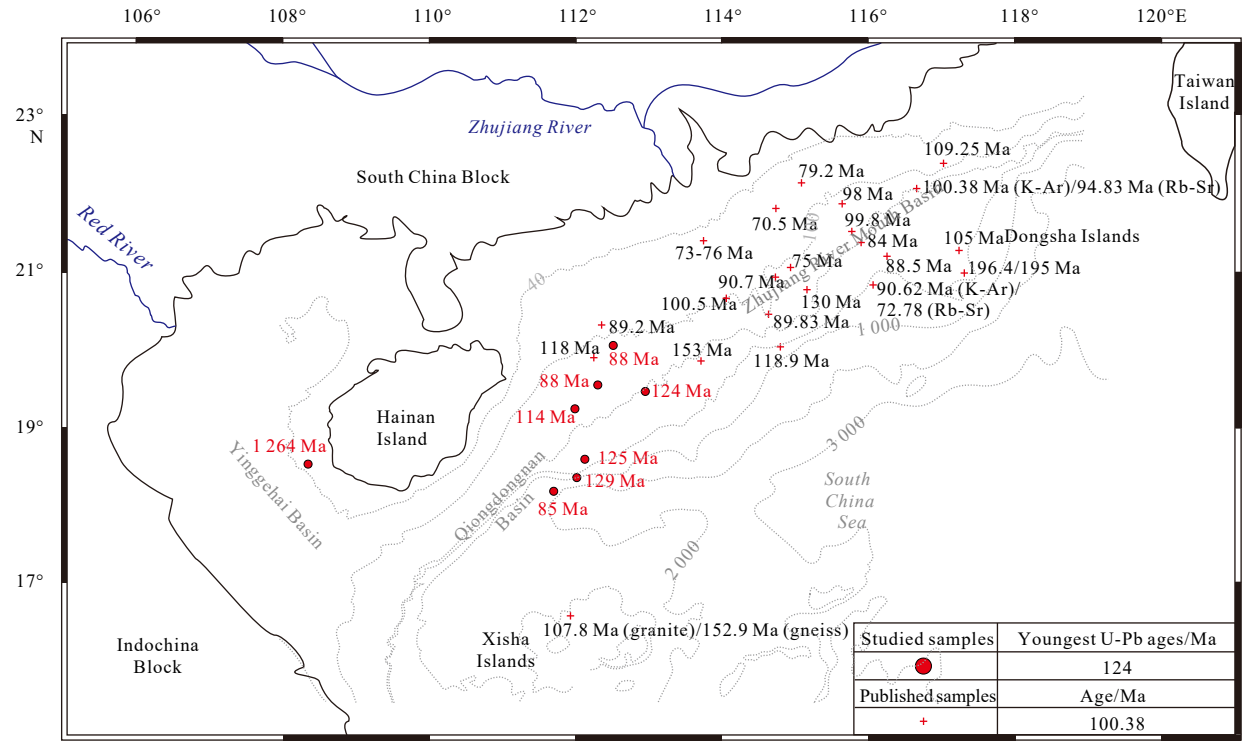

Fig. 8. Distribution map of the youngest ages dated by detrital zircon U-Pb ages for the studied meta-clastic rock samples, and K-Ar or Rb-Sr ages of previous researches for the northern SCS Basin basement.

Pubellier et al. (2008)). To be more detailed, RTP magnetic anomalies can effectively pinpoint the Mesozoic sedimentary deposition, which has extremely low-magnetic susceptibility. This parameter is also suited for late-stage magmatism detection. A high-value anomaly belt with NE trending is developed on Fig. 9a, which roughly corresponds to the Dongsha basement high and the strong Mesozoic magmatic activities (Li et al., 2008a, 2008b). Patches of obvious magnetic quiescence, on the other hand, are also recognized within the eastern SCS. They are possibly related to the residual distributions of thick Mesozoic sedimentary strata. Comparatively, the free-air gravity map shows that a relatively high-anomaly zone develops around the Dongsha Islands of the eastern SCS. The free-air gravity pattern is in line with the RTP magnetic anomalies. Briefly, both of these data highs are likely to be caused by Mesozoic magmatic events. However, low-gravity anomalies are also sparsely displayed along the high-anomaly magmatic belt mentioned above (Fig. 9b). This could be interpreted as the existence of a fault and sag zone, which was formed adjacent to the Dongsha igneous bodies. Partly within the eastern SCS region, it might be a little contradictory to find that, higher gravity-anomaly values (between –5 mGal and 10 mGal) are linked to relatively lower RTP magnetic anomalies. In this regard, this observation suggests that these areas are possibly basement uplifts mainly comprised of Mesozoic sedimentary bodies. Con-

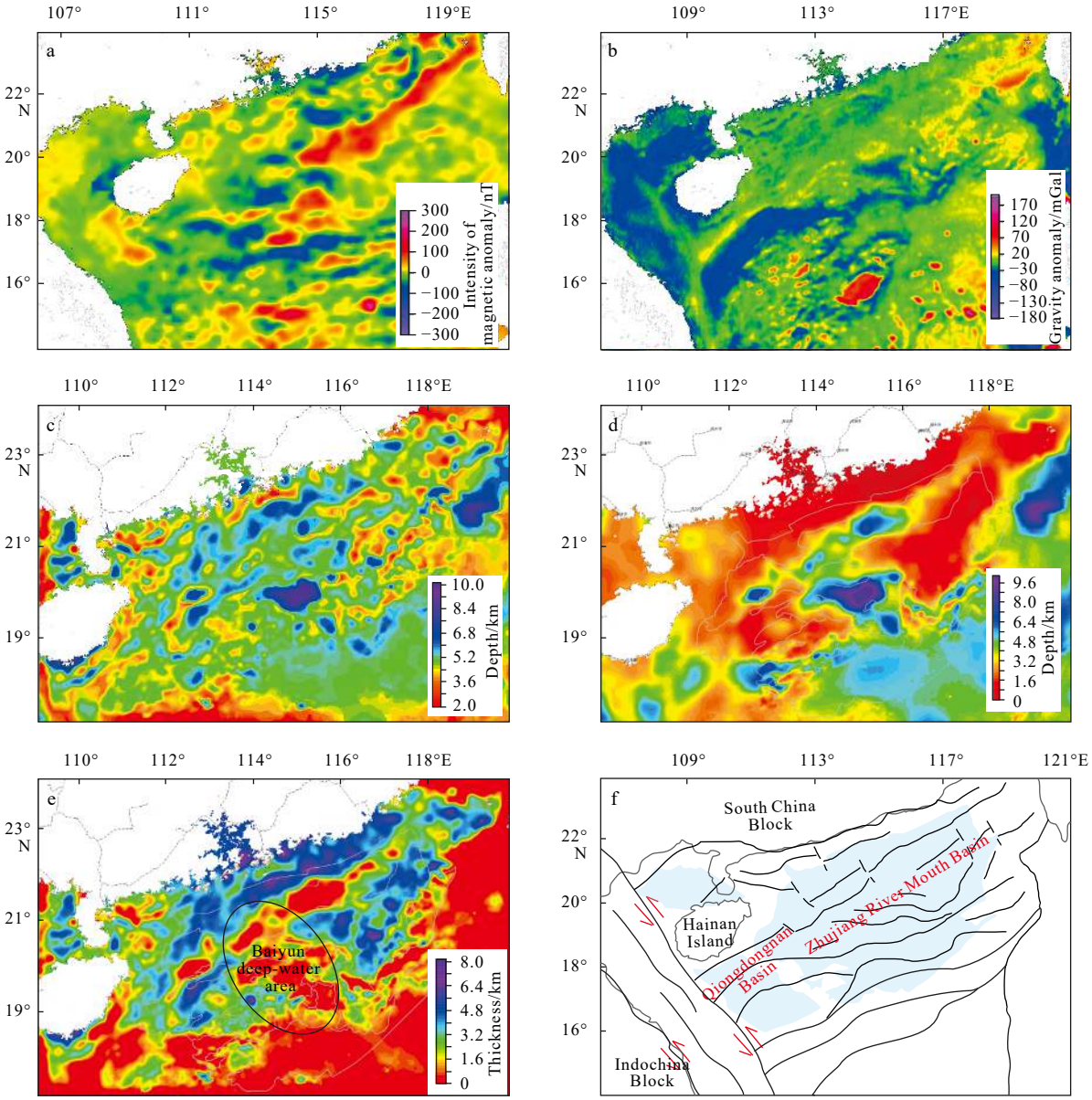

Fig. 9. Map of magnetic anomalies after reduction to the pole to precisely relocate magnetic boundaries and facilitates data interpretation (a); regional free-air gravity anomaly map based on high-resolution shipborne surveying and satellite measurements offshore (b) (Sandwell and Smith, 1997); regional bathymetrical map showing the bottom layer of the pre-Cenozoic basement based on gravity-magnetic-seismic joint inversion, assuming an average of 2.67 g/cm^3 for shallow crustal materials (c); regional bathymetrical map showing the bottom layer of the Cenozoic sedimentary sequences (d); thickness reconstruction map of the northern South China Sea pre-Cenozoic sedimentary basin basement (e); sketch map showing the SCS Basin basement tectonic units and major faults (f). Dash lines are faults which are drawn based on both gravity-magnetic-seismic anomaly interpretations in this study and published geological data (modified from Pubellier et al. (2008)).

strained by the precise dating of our penetrations and previous studies, the SCS basement is more reasonable to be described as an overall Mesozoic stratigraphic framework instead of a faulting-division system.

It should also be dealt with much precaution for the westernmost metamorphic granite sample Y1 on the eastern margin of Yinggehai Basin (Fig. 1a). The prominent single peak of significantly old Precambrian age makes it distinct from other results (Fig. 6c). The typical directional-alignment textures indicate a relatively stronger metamorphism under crossed polarized microscope (Figs 7g and h). However, zircon grains of metamorphic origin were unlikely to be practically produced in light of their Th/U ratios (> 0.1) as well as oscillatory-zoning crystal structures. Based on a review of related literature, the Mesozoic SCS region was well-known to be controlled under a drastically changing tectonic background (Hall, 2002, 2012; Zhou et al., 2008; Li et al., 2012). This area is supposed to have experienced an episode of Meso-Tethys and Paleo-Pacific interactions where drastic subduction, collision as well as suturing continually took place (Fig. 10). Under the active Paleo-Pacific subduction geological setting, abundant Cretaceous ages for granite intrusive bodies gathering around the eastern SCS region indeed provide direct lines of evidence for the Mesozoic magmatic arc along the continental margin (Table 1, Fig. 8). Comparatively, meta-clastic rocks with Mesozoic ages (mainly early Cretaceous) are dominant of presence in the eastern Hainan Basin, the western SCS (Fig. 8). Further west, the Indochina Block has been continually colliding with the Cathaysian Landmass during the late Triassic (Roger et al., 2000; Lepvrier et al., 2004, 2008). The fact that Y1 lies coincidentally along the Red River Fault Zone strongly indicates large-scale preservation of the old continental relicts during this suite of continental collisions and Tethyan suffocation processes. These ancient records might be largely related to the Gondwana-land-derived Indochina Block, as suggested from metamorphic granite Y1 and the old basement of Hainan Island. To a certain degree, it further confirms potential provenances of Proterozoic or Paleozoic materials for the minor age populations in the studied metamorphic sedimentary samples (Fig. 6b).

Fairly homogeneous properties are recognized across the western Zhujiang River Mouth Basin as well as Qiongdongnan Basin based on the magnetic and gravity anomalies (Figs 9a and b). On the RTP map, a near-uniform distribution pattern is observed with moderately negative to slightly positive magnetic anomalies. Clear dividing boundaries are not identified for the extensive quiet magnetic zones of Mesozoic sediments. To be noted, Yinggehai Basin displays conspicuously negative gravity anomalies, which is in contrast with the wide distribution of medium-value positive anomalies to the east of Hainan Island (Fig. 9b). It is postulated to be physical property distinction as confirmed by petrographic and geochronological evidences. Furthermore, the 2D thickness reconstruction map of the pre-Cenozoic strata has been obtained as shown in Fig. 9e. It was achieved by subtracting the Cenozoic sedimentary cover from the total Mesozoic-upward sequences (Figs 9c and d). It reveals that the Mesozoic strata are generally distributed in the western SCS region, east of Hainan Island. With regard to the Baiyun deep-water area, the

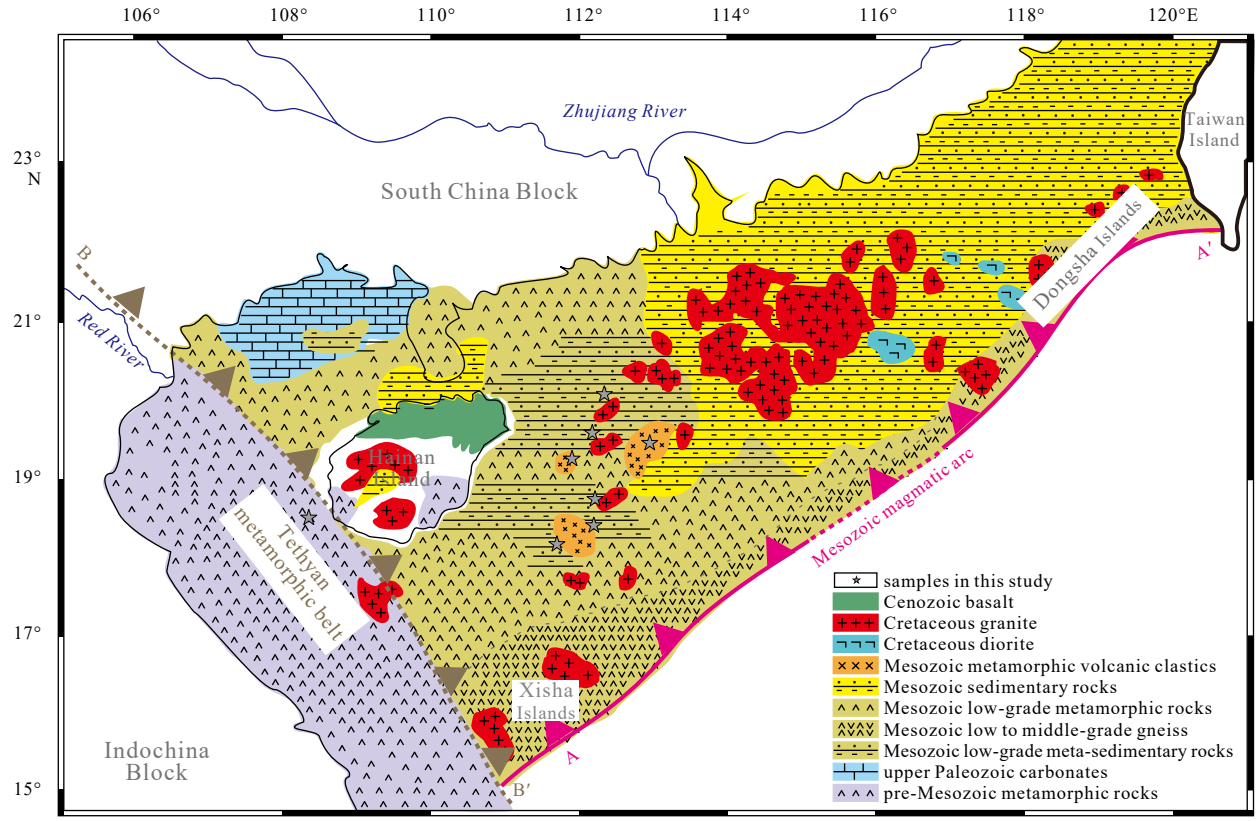

Fig. 10. Systematic northern SCS pre-Cenozoic basement lithological map with an interpreted Mesozoic magmatic arc A-A' shown along the continental margin. This lithological pattern is constrained by the new ages, geochemical analysis, petrographic slice observation and gravity-magnetic-seismic joint inversion results reported in this study as well as other published data (Qiu et al., 1996; Li et al., 1999; Xu et al., 2017). A postulated Tethyan subduction direction is also shown to the west of Hainan Island. Section B-B' shows the possible active boundary of the pre-Cenozoic metamorphic belt along the present extension of the Red River Fault Zone (modified from Wang et al. (2002) and Sun et al. (2014)).

obviously thinning basement could possibly be explained by the relationship between crustal stretching and basin structure (Fig. 9e). During the early stage of the syn-rifting period, the Baiyun deep-water area was mainly influenced from the brittle extension of the upper crust. When it came to the late stage of the syn-rifting period, the strongly crustal ductile deformation caused a saucer-shaped rheology change. After eliminating the influence from the overlying sedimentary sequences, it seems that the depths of Moho and SCS sedimentary basin basement are displayed as mirrorimage relationship (Pang et al., 2018; Lei et al., 2019a). In any case, the sketched tectonic-unit reconstruction firstly attempts to show that the northern SCS Basin basement was formed under the mechanism of spatially uniform stress-field (Fig. 9f).

5.3 *SCS Basin basement evolution and regional geodynamic implications*

From at least late Triassic to early Cretaceous, the SCS area has been influenced from both Meso-Tethys and Paleo-Pacific domains (Metcalfe, 1996; Carter et al., 2001; Hall, 2002, 2012; Zhou et al., 2008). The southeastern Eurasian margin has been experiencing a very complicated evolutional history (Lei et al., 2019a) (Fig. 11a). The lack of basinal evidence has led to misleading interpretations on the pre-Cenozoic SCS basement prior to the subsequent generation of Tertiary oceanic basins. The newly obtained zircon U-Pb ages, elemental geochemistry and petrographic identification commonly provide significant constraints on the pre-Cenozoic SCS basement as well as geodynamic evolution of the Southeast Asia. From late Triassic to early Jurassic, a Meso-Tethyan subduction environment was likely to exist between the Indochina Block and Cathysian Block extending from the northwest to southeast (Roger et al., 2000; Lepvrier et al., 2004, 2008; Sone and Metcalfe, 2008) (Fig. 11b). As a separate micro-continental terrane, the original structure of the Hainan Island (or considered as "proto-Hainan Island") was likely to have occurred within the front of Meso-Tethyan subduction under this overall compressional tectonic setting. Although the final amalgamation remains unclear on its precise timing, formation of Hainan Island can be considered as a part of accretionary prism during the drastic intercontinental collision. With respect to the NE–SW trending of stronger metamorphism over the broad SCS Basin basement, the Indochina Block might have been driven for continual collision and deformation with the Cathaysia during the whole Mesozoic. These long-lasting subduction processes undoubtedly led to stronger contact metamorphism between rigid continental terranes. From late Jurassic to early Cretaceous (Fig. 11c), the Paleo-Pacific subduction system kept affecting the SCS area to the east, which led to the development of the Andean-type continental margin. With the Paleo-Pacific Plate subducting under the South China Block, a series of large-scale magmatic and orogenic movements took place within the South China during the late Mesozoic (Zhou and Li, 2000; Zhou et al., 2006). The acceleration of subduction also resulted in broader arc magmatism and accompanied back-arc extensional basins when it turned to late Jurassic–early Cretaceous. The oceanic-continental collision has caused relatively weaker metamorphism in the eastern area of the northern SCS Basin basement. Compared to the more complicated and intense metamorphism to the west of Hainan Island, influence from the Paleo-Pacific subduction system seems limited by resulting in narrower and weaker metamorphic belt (Fig. 10). Away from the subduction zone, metamorphism tends to be sharply weakened from south to further north. It should also be noted that Xisha area might be sequentially influenced from multi-stage collisions of both the Indochina Block and Paleo-Pacific. As the significant intersection of the northern SCS Basin basement, a more intense and extensive metamorphic belt has been possibly generated under these different geotectonic domains.

6 Conclusions

Geochemical analyses, petrographic identification, detrital zircon U-Pb geochronology as well as geophysical constraints from gravity-magnetic joint inversion have been conducted on the northern SCS pre-Cenozoic basement samples. In this study, it is reinterpreted that the pre-Cenozoic crustal structure is actually dominated by the widespread distribution of Mesozoic strata, rather than a matching basement of heterogeneous segments. Corroborated from the previous U-Pb, K-Ar and Rb-Sr Cretaceous isochron ages on granite intrusives within the northeastern SCS region, it is proposed that the regional magmatic arc surrounding the South China continental margin was under con-

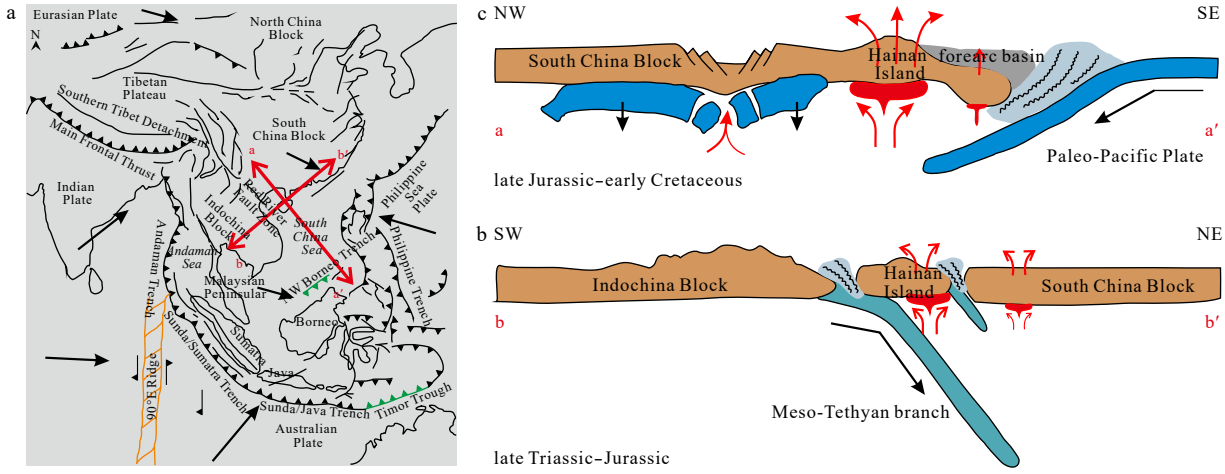

Fig. 11. Sketch map showing the present topographic and active faults of the east Asia at the convergence zone of the Eurasian Plate, Philippine Sea Plate and Australian-Indian Plate (a) (modified from Metcalfe (1996, 2011)). A cartoon illustrating the switch-on and switch-off evolution of the Meso-Tethyan tectonic regime in the late Triassic–Jurassic (b) and the Paleo-Pacific regime in the late Jurassic–early Cretaceous (c).

trol from the drastic Paleo-Pacific subduction. Displaying depositional ages of late Jurassic to Cretaceous, the studied tuff and volcaniclastic rock samples suggest a western extension of this active magmatic belt. A suite of meta-clastic rock samples to the east of Hainan Island, the western SCS, have also been examined indicating the existence of a low-grade metamorphosed Mesozoic basement. Bimodal patterns of Yanshanian and Caledonian peaks in part of the studied samples suggest provenances consisting of Mesozoic and Paleozoic zircon grains. Finally, located on the Red River Fault Zone, the metamorphic granites with Precambrian zircon ages imply extensive preservation of ancient continental landmasses during the subduction, collision and uplifting activities between the Indochina Block and Cathaysian Block. In fact, the Red River Fault Zone could be considered as the reactivation of the suturing belt along these contiguous plate margins during the Cenozoic. Tectonically, the Hainan Island is actually regarded to be part of the accretionary complex on the continental boundaries. Apparently, the northern SCS Basin basement was practically generated from both intracontinental amalgamation and oceanic-continental collision processes. The Tertiary SCS oceanic basin was finally developed from a series of rifting and faulting along the collisional-accretionary continental margin.

Acknowledgements

We thank China National Offshore Oil Corporation (CNOOC) for providing geological data and borehole samples from the northern South China Sea basement. Reviewers and guest editors offered critical comments and suggestions, which greatly improved this presentation. Yuchi Cui acknowledges the China Scholarship Council and Curtin CIPRS for providing research scholarship for her Joint PhD study at Curtin University.

References

Andersen T. 2002. Correction of common lead in U-Pb analyses that do not report ^{204}Pb. Chemical Geology, 192(1–2): 59–79

Barckhausen U, Engels M, Franke D, et al. 2014. Evolution of the South China Sea: Revised ages for breakup and seafloor spreading. Marine and Petroleum Geology, 58: 599–611, doi: 10.1016/j.marpetgeo.2014.02.022

Braitenberg C, Wienecke S, Wang Yong. 2006. Basement structures from satellite-derived gravity field: South China Sea ridge. Journal of Geophysical Research, 111(B5): B05407

Briais A, Patriat P, Tapponnier P. 1993. Updated interpretation of magnetic anomalies and seafloor spreading stages in the South China Sea: implications for the Tertiary Tectonics of Southeast Asia. Journal of Geophysical Research, 98(B4): 6299–6328, doi: 10.1029/92JB02280

Cao Licheng, Shao Lei, Qiao Peijun, et al. 2018. Early Miocene birth of modern Pearl River recorded low-relief, high-elevation surface formation of SE Tibetan Plateau. Earth and Planetary Science Letters, 496: 120–131, doi: 10.1016/j.epsl.2018.05.039

Carter A, Roques D, Bristow C, et al. 2001. Understanding Mesozoic accretion in Southeast Asia: Significance of Triassic thermotectonism (Indosinian orogeny) in Vietnam. Geology, 29(3): 211–214, doi: 10.1130/0091-7613(2001)029<0211:UMAISA>2.0.CO;2

Charvet J, Shu Liangshu, Faure M, et al. 2010. Structural development of the Lower Paleozoic belt of South China: genesis of an intracontinental orogen. Journal of Asian Earth Sciences, 39(4): 309–330, doi: 10.1016/j.jseaes.2010.03.006

Clift P, Lin Jian. 2001. Preferential mantle lithospheric extension under the South China margin. Marine and Petroleum Geology, 18(8): 929–945, doi: 10.1016/S0264-8172(01)00037-X

Cocks L R M, Torsvik T H. 2013. The dynamic evolution of the Palaeozoic geography of eastern Asia. Earth-Science Reviews, 117: 40–79, doi: 10.1016/j.earscirev.2012.12.001

Dien P T, Nielsen L H, Andersen C, et al. 1998. Late-Mesozoic and Cenozoic basin development along the northwest margin of Vietnam. In: American Association of Petroleum Geologists Annual Convention. Salt Lake City, UT, USA: American Association of Petroleum Geologisits, 1–6, doi: 10.1306/00AA84F4-1730-11D7-8645000102C1865D.

Ebbing J, Braitenberg C, Götze H J. 2006. The lithospheric density structure of the Eastern Alps. Tectonophysics, 414(1–4): 145–155

Ebinger C J, Hayward N J. 1996. Soft plates and hot spots: Views from afar. Journal of Geophysical Research, 101(B10): 21859–21876, doi: 10.1029/96JB02118

Faure M, Lepvrier C, Van Nguyen V, et al. 2014. The South China block-Indochina collision: Where, when, and how?. Journal of Asian Earth Sciences, 79: 260–274, doi: 10.1016/j.jseaes.2013.09.022

Faure M, Lin Wei, Chu Yang, et al. 2016. Triassic tectonics of the southern margin of the South China Block. Comptes Rendus Geoscience, 348(1): 5–14, doi: 10.1016/j.crte.2015.06.012

Franke D, Barckhausen U, Baristeas N, et al. 2011. The continent-ocean transition at the southeastern margin of the South China Sea. Marine and Petroleum Geology, 28(6): 1187–1204, doi: 10.1016/j.marpetgeo.2011.01.004

Fyhn M B W, Cuong T D, Hoang B H, et al. 2018. Linking Paleogene rifting and inversion in the northern Song Hong and Beibuwan Basins, Vietnam, with left-lateral motion on the Ailao Shan-Red River Shear Zone. Tectonics, 37(8): 2559–2585, doi: 10.1029/2018TC005090

Geological Survey of Japan and Coordinating Committee for Coastal and Offshore Geoscience Programmes in East and Southeast Asia (CCOP). 1996. Magnetic Anomaly Map of East Asia 1: 4, 000, 000. Tsukuba-shi, Ibaraki-ken: The Survey

Hall R. 2002. Cenozoic geological and plate tectonic evolution of SE Asia and the SW Pacific: computer-based reconstructions, model and animations. Journal of Asian Earth Sciences, 20(4): 353–431, doi: 10.1016/S1367-9120(01)00069-4

Hall R. 2012. Late Jurassic-Cenozoic reconstructions of the Indonesian region and the Indian Ocean. Tectonophysics, 570–571: 1–41

Hao Tianyao, Xu Ya, Sun Fuli, et al. 2011. Integrated geophysical research on the tectonic attribute of conjugate continental margin of South China Sea. Chinese Journal of Geophysics (in Chinese), 54(12): 3098–3116

Hayes D E, Nissen S S. 2005. The South China sea margins: Implications for rifting contrasts. Earth and Planetary Science Letters, 237(3–4): 601–616

Hoskin P W O, Schaltegger U. 2003. The composition of zircon and igneous and metamorphic petrogenesis. Reviews in Mineralogy and Geochemistry, 53(1): 27–62, doi: 10.2113/0530027

Hsu S K, Yeh Y C, Doo W B, et al. 2004. New bathymetry and magnetic lineations identifications in the northernmost South China Sea and their tectonic implications. Marine Geophysical Researches, 25(1–2): 29–44

Hutchison C S. 1989. Geological evolution of South-east Asia. In: Oxford Monographs on Geology and Geophysics. Oxford, England: Clarendon Press, 368

Jahn B M, Zhou Xinhua, Li Jiliang. 1990. Formation and tectonic evolution of Southeastern China and Taiwan: Isotopic and geochemical constraints. Tectonophysics, 183(1–4): 145–160

Jiang Xiaoyan, Li Xianhua, Collins W J, et al. 2015. U-Pb age and Hf-O isotopes of detrital zircons from Hainan Island: Implications for Mesozoic subduction models. Lithos, 239: 60–70, doi: 10.1016/j.lithos.2015.10.006

Lan C Y, Chung S L, Van Long T, et al. 2003. Geochemical and Sr–Nd isotopic constraints from the Kontum massif, central Vietnam on the crustal evolution of the Indochina block. Precambrian Research, 122(1–4): 7–27

Lapierre H, Jahn B M, Charvet J, et al. 1997. Mesozoic felsic arc magmatism and continental olivine tholeiites in Zhejiang Province and their relationship with the tectonic activity in southeastern China. Tectonophysics, 274(4): 321–338, doi: 10.1016/S0040-1951(97)00009-7

Larsen H C, Mohn G, Nirrengarten M, et al. 2018. Rapid transition from continental breakup to igneous oceanic crust in the South China Sea. Nature Geoscience, 11(10): 782–789, doi: 10.1038/

s41561-018-0198-1
Lei Chao, Alves T M, Ren Jianye, et al. 2019a. Depositional architecture and structural evolution of a region immediately inboard of the locus of continental breakup (Liwan Sub-basin, South China Sea). GSA Bulletin, 131(7–8): 1059–1074, doi: 10.1130/B35001.1
Lei Chao, Clift P D, Ren Jianye, et al. 2019b. A rapid shift in the sediment routing system of Lower-Upper Oligocene strata in the Qiongdongnnan Basin (Xisha Trough), Northwest South China Sea. Marine and Petroleum Geology, 104: 249–258, doi: 10.1016/j.marpetgeo.2019.03.012
Lei Chao, Ren Jianye. 2016. Hyper-extended rift systems in the Xisha Trough, northwestern South China Sea: Implications for extreme crustal thinning ahead of a propagating ocean. Marine and Petroleum Geology, 77: 846–864, doi: 10.1016/j.marpetgeo.2016.07.022
Lei Chao, Ren Jianye, Pang Xiong, et al. 2018. Continental rifting and sediment infill in the distal part of the northern South China Sea in the Western Pacific region: Challenge on the present-day models for the passive margins. Marine and Petroleum Geology, 93: 166–181, doi: 10.1016/j.marpetgeo.2018.02.020
Leloup P H, Arnaud N, Lacassin R, et al. 2001. New constraints on the structure, thermochronology, and timing of the Ailao Shan-Red River shear zone, SE Asia. Journal of Geophysical Research, 106(B4): 6683–6732, doi: 10.1029/2000JB900322
Lepvrier C, Maluski H, Van Tich V, et al. 2004. The Early Triassic Indosinian orogeny in Vietnam (Truong Son Belt and Kontum Massif); implications for the geodynamic evolution of Indochina. Tectonophysics, 393(1–4): 87–118
Lepvrier C, Van Vuong N, Maluski H, et al. 2008. Indosinian tectonics in Vietnam. Comptes Rendus Geoscience, 340(2–3): 94–111
Li Chunfeng, Zhou Zuyi, Hao Hujun, et al. 2008a. Late Mesozoic tectonic structure and evolution along the present-day northeastern South China Sea continental margin. Journal of Asian Earth Sciences, 31(4–6): 546–561
Li Chunfeng, Zhou Zuyi, Li Jiabiao, et al. 2008b. Magnetic zoning and seismic structure of the South China Sea ocean basin. Marine Geophysical Researches, 29(4): 223–238, doi: 10.1007/s11001-008-9059-4
Li Jianhua, Zhang Yueqiao, Dong Shuwen, et al. 2014. Cretaceous tectonic evolution of South China: A preliminary synthesis. Earth-Science Reviews, 134: 98–136, doi: 10.1016/j.earscirev.2014.03.008
Li Pinglu, Liang Huixian, Dai Yiding, et al. 1999. Origin and tectonic setting of the Yanshanian igneous rocks in the Pearl River Mouth Basin. Guangdong Geology (in Chinese), 14(1): 1–8
Li Sanzhong, Zhang Guowei, Zhou Lihong, et al. 2011. The opposite Meso-Cenozoic intracontinental deformations under the super-convergence: Rifting and extension in the North China Craton and shortening and thrusting in the South China Craton. Earth Science Frontiers (in Chinese), 18(3): 79–107
Li Xianhua, Li Zhengxiang, Li Wuxian, et al. 2006. Initiation of the Indosinian orogeny in South China: Evidence for a Permian magmatic arc on Hainan Island. The Journal of Geology, 114(3): 341–353, doi: 10.1086/501222
Li Xianhua, Wei Gangjian, Shao Lei, et al. 2003. Geochemical and Nd isotopic variations in sediments of the South China Sea: a response to Cenozoic tectonism in SE Asia. Earth and Planetary Science Letters, 211(3–4): 207–220
Li Zhengxiang, Li Xianhua. 2007. Formation of the 1300-km-wide intracontinental orogen and postorogenic magmatic province in Mesozoic South China: A flat-slab subduction model. Geology, 35(2): 179–182, doi: 10.1130/G23193A.1
Li Zhengxiang, Li Xianhua, Chung S L, et al. 2012. Magmatic switch-on and switch-off along the South China continental margin since the Permian: Transition from an Andean-type to a Western Pacific-type plate boundary. Tectonophysics, 532–535: 271–290
Li Zhengxiang, Li Xianhua, Li Wuxian, et al. 2008c. Was Cathaysia part of Proterozoic Laurentia?—New data from Hainan Island, South China. Terra Nova, 20(2): 154–164, doi: 10.1111/j.1365-3121.2008.00802.x
Li Zhengxiang, Powell C M. 2001. An outline of the palaeogeographic evolution of the Australasian region since the beginning of the Neoproterozoic. Earth-Science Reviews, 53(3–4): 237–277
Liu Hailing, Yan Pin, Liu Yingchun, et al. 2006. Existence of Qiongnan suture zone on the north margin of South China Sea. Chinese Science Bulletin, 51(S2): 107–120, doi: 10.1007/s11434-006-9107-x
Liu Hailing, Zheng Hongbo, Wang Yanlin, et al. 2011. Basement of the South China Sea area: Tracing the Tethyan realm. Acta Geologica Sinica, 85(3): 637–655, doi: 10.1111/j.1755-6724.2011.00457.x
Liu Yongsheng, Gao Shan, Hu Zhaochu, et al. 2010. Continental and oceanic crust recycling-induced melt-peridotite interactions in the trans-north China orogen: U-Pb dating, Hf isotopes and trace elements in zircons from mantle xenoliths. Journal of Petrology, 51(1–2): 537–571
Lu Baoliang, Sun Xiaomeng, Zhang Gongcheng, et al. 2011. Seismic-potential field response characteristics and identification of basement lithology of the northern South China Sea basin. Chinese Journal of Geophysics (in Chinese), 54(2): 563–572
Maruyama S. 1997. Pacific-type orogeny revisited: Miyashiro-type orogeny proposed. Island Arc, 6(1): 91–120, doi: 10.1111/j.1440-1738.1997.tb00042.x
Metcalfe I. 1996. Gondwanaland dispersion, Asian accretion and evolution of eastern Tethys. Australian Journal of Earth Sciences, 43(6): 605–623, doi: 10.1080/08120099608728282
Metcalfe I. 2011. Palaeozoic-Mesozoic history of SE Asia. In: Geological Society London Special Publications. London: The Geological Society of London, 355(1): 7–35, doi: 10.1144/SP355.2
Metcalfe I. 2013. Gondwana dispersion and Asian accretion: Tectonic and palaeogeographic evolution of eastern Tethys. Journal of Asian Earth Sciences, 66: 1–33, doi: 10.1016/j.jseaes.2012.12.020
Morley C K. 2002. A tectonic model for the Tertiary evolution of strike-slip faults and rift basins in SE Asia. Tectonophysics, 347(4): 189–215, doi: 10.1016/S0040-1951(02)00061-6
Morley C K. 2012. Late cretaceous-Early Palaeogene tectonic development of SE Asia. Earth-Science Reviews, 115(1–2): 37–75
Morley C K. 2016. Major unconformities/termination of extension events and associated surfaces in the South China seas: Review and implications for tectonic development. Journal of Asian Earth Sciences, 120: 62–86, doi: 10.1016/j.jseaes.2016.01.013
Nielsen L H, Mathiesen A, Bidstrup T, et al. 1999. Modelling of hydrocarbon generation in the Cenozoic Song Hong Basin, Vietnam: a highly prospective basin. Journal of Asian Earth Sciences, 17(1–2): 269–294
Nissen S S, Hayes D E, Buhl P, et al. 1995a. Deep penetration seismic soundings across the northern margin of the South China Sea. Journal of Geophysical Research, 100(B11): 22407–22433, doi: 10.1029/95JB01866
Nissen S S, Hayes D E, Yao Bochu, et al. 1995b. Gravity, heat flow, and seismic constraints on the processes of crustal extension: Northern margin of the South China Sea. Journal of Geophysical Research, 100(B11): 22447–22483, doi: 10.1029/95JB01868
Pang Xiong, Ren Jianye, Zheng Jinyun, et al. 2018. Petroleum geology controlled by extensive detachment thinning of continental margin crust: A case study of Baiyun sag in the deep-water area of northern South China Sea. Petroleum Exploration and Development (in Chinese), 45(1): 27–39
Pearce J A. 1983. Role of the sub-continental lithosphere in magma genesis at active continental margins. In: Hawkesworth C J, Norry M J, eds. Continental Basalts and Mantle Xenoliths. Nantwich: Shiva Publishing, 230–249
Pearce J A, Peate D W. 1995. Tectonic implications of the composition of volcanic arc magmas. Annual Review of Earth and Planetary Sciences, 23: 251–285, doi: 10.1146/annurev.ea.23.050195.001343
Pichot T, Delescluse M, Chamot-Rooke N, et al. 2014. Deep crustal structure of the conjugate margins of the SW South China Sea from wide-angle refraction seismic data. Marine and Petroleum Geology, 58: 627–643, doi: 10.1016/j.marpetgeo.2013.10.008
Pigott J D, Ru Ke. 1994. Basin superposition on the northern margin of the South China Sea. Tectonophysics, 235(1–2): 27–50
Pubellier M, Chamot-Rooke N, Ego F, et al. 2008. Structural map of eastern Eurasia, scale 1/12 500 000. Paris: Commission for the Geological Map of the World

Qin Guoquan. 1987. A preliminary study on foraminiferal assemblages of well 1 Xiyong. Xisha Islands and their coral reef formation. Tropic Oceanology (in Chinese), 6(3): 10–20
Qiu Xuelin, Ye Sanyu, Wu Shimin, et al. 2001. Crustal structure across the Xisha Trough, northwestern South China Sea. Tectonophysics, 341(1–4): 179–193
Qiu Yuanxi, Li Pinglu, Liang Huixian. 1996. Late Cretaceous-Cenozoic tectonic evolution and nature of continental margin in the northern South China Sea and Taiwan Strait. Guangdong Geology (in Chinese), 11(3): 10–16
Rangin C, Klein M, Roques D, et al. 1995. The Red River fault system in the Tonkin Gulf, Vietnam. Tectonophysics, 243(3–4): 209–222
Roger F, Leloup P H, Jolivet M, et al. 2000. Long and complex thermal history of the Song Chay metamorphic dome (Northern Vietnam) by multi-system geochronology. Tectonophysics, 321(4): 449–466, doi: 10.1016/S0040-1951(00)00085-8
Rudnick R L, Gao Shan. 2003. The composition of the continental crust. In: Holland HD, Turekian KK, eds. Treatise on Geochemistry. Oxford: Elsevier-Pergamon, 1–64
Sandwell D T, Smith W H F. 1997. Marine gravity anomaly from Geosat and ERS 1 satellite altimetry. Journal of Geophysical Research, 102(B5): 10039–10054, doi: 10.1029/96JB03223
Schellart W P, Lister G S, Toy V G. 2006. A Late Cretaceous and Cenozoic reconstruction of the southwest Pacific region: Tectonics controlled by subduction and slab rollback processes. Earth-Science Reviews, 76(3–4): 191–233
Shao Lei, Cao Licheng, Pang Xiong, et al. 2016. Detrital zircon provenance of the Paleogene syn-rift sediments in the northern South China Sea. Geochemistry, Geophysics, Geosystems, 17(2): 255–269, doi: 10.1002/2015GC006113
Shao Lei, Cao Licheng, Qiao Peijun, et al. 2017. Cretaceous–Eocene provenance connections between the Palawan Continental Terrane and the northern South China Sea margin. Earth and Planetary Science Letters, 477: 97–107, doi: 10.1016/j.epsl.2017.08.019
Shao Lei, Cui Yuchi, Stattegger K, et al. 2019. Drainage control of Eocene to Miocene sedimentary records in the southeastern margin of Eurasian Plate. GSA Bulletin, 131(3–4): 461–478
Shao Lei, Qiao Peijun, Zhao Meng, et al. 2015. Depositional style of the northern South China Sea between Oligocene and Miocene in response to the evolution of the Pearl River. In: Clift P D, Harff J, Wu J, et al, eds. River-Dominated Shelf Sediments of East Asian Seas. London: The Geological Society of London
Shi Hesheng, Li Chunfeng. 2012. Mesozoic and early Cenozoic tectonic convergence-to-rifting transition prior to opening of the South China Sea. International Geology Review, 54(15): 1801–1828, doi: 10.1080/00206814.2012.677136
Sláma J, Košler J, Condon D J, et al. 2008. Plešovice zircon—A new natural reference material for U-Pb and Hf isotopic microanalysis. Chemical Geology, 249(1–2): 1–35
Sone M, Metcalfe I. 2008. Parallel Tethyan sutures in mainland Southeast Asia: New insights for Palaeo-Tethys closure and implications for the Indosinian orogeny. Comptes Rendus Geoscience, 340(2–3): 166–179, doi: 10.1016/j.crte.2007.09.008
Sun S S, McDonough W F. 1989. Chemical and isotopic systematics of oceanic basalts: Implications for mantle composition and processes. London: The Geological Society of London, 42(1): 313–345, doi: 10.1144/GSL.SP.1989.042.01.19
Sun Xiaomeng, Zhang Xuqing, Zhang Gongcheng, et al. 2014. Texture and tectonic attribute of Cenozoic basin basement in the northern South China Sea. Science China: Earth Sciences, 57(6): 1199–1211, doi: 10.1007/s11430-014-4835-2
Taylor S R, McLennan S M. 1985. The Continental Crust: Its Composition and Evolution. Oxford: Blackwell Scientific Publications, 1–312
Veevers J J. 2004. Gondwanaland from 650–500 Ma assembly through 320 Ma merger in Pangea to 185–100 Ma breakup: supercontinental tectonics via stratigraphy and radiometric dating. Earth-Science Reviews, 68(1–2): 1–132
Vermeesch P. 2012. On the visualisation of detrital age distributions. Chemical Geology, 312–313: 190–194
Vượng N V, Hansen B T, Wemmer K, et al. 2013. U/Pb and Sm/Nd dating on ophiolitic rocks of the Song Ma suture zone (northern Vietnam): Evidence for Upper Paleozoic Paleotethyan lithospheric remnants. Journal of Geodynamics, 69: 140–147, doi: 10.1016/j.jog.2012.04.003
Wallace L M, Ellis S, Miyao K, et al. 2009. Enigmatic, highly active left-lateral shear zone in southwest Japan explained by aseismic ridge collision. Geology, 37(2): 143–146, doi: 10.1130/G25221A.1
Wan Ling, Yao Bochu, Zeng Weijun, et al. 2006. Lithospheric structure and petroleum distribution in the South China Sea. Geology in China (in Chinese), 33(4): 874–884
Wang Jialin, Zhang Xinbing, Wu Jiansheng, et al. 2002. Integrated geophysical researches on base texture of Zhujiang River Mouth basin. Journal of Tropical Oceanography (in Chinese), 21(2): 13–22
Wang Yuejun, Zhang Aimei, Fan Weiming, et al. 2011. Kwangsian crustal anatexis within the eastern South China Block: Geochemical, zircon U-Pb geochronological and Hf isotopic fingerprints from the gneissoid granites of Wugong and Wuyi-Yunkai Domains. Lithos, 127(1–2): 239–260
Wei Gangjian, Li Xianhua, Liu Ying, et al. 2006. Geochemical record of chemical weathering and monsoon climate change since the early Miocene in the South China Sea. Paleoceanography, 21(4): PA4214, doi: 10.1029/2006PA001300
Wiedenbeck M, Allé P, Corfu F, et al. 1995. Three natural zircon standards for U-Th-Pb, Lu-Hf, trace element and REE analyses. Geostandards and Geoanalytical Research, 19(1): 1–23, doi: 10.1111/j.1751-908X.1995.tb00147.x
Xu Changhai, Zhang Lu, Shi Hesheng, et al. 2017. Tracing an early Jurassic magmatic arc from South to East China Seas. Tectonics, 36(3): 466–492, doi: 10.1002/2016TC004446
Xu Deru, Xia Bin, Bakun-Czubarow N, et al. 2008. Geochemistry and Sr-Nd isotope systematics of metabasites in the Tunchang area, Hainan Island, South China: implications for petrogenesis and tectonic setting. Mineralogy and Petrology, 92(3): 361–391
Yan Quanshu, Shi Xuefa, Liu Jihua, et al. 2010. Petrology and geochemistry of Mesozoic granitic rocks from the Nansha microblock, the South China Sea: Constraints on the basement nature. Journal of Asian Earth Sciences, 37(2): 130–139, doi: 10.1016/j.jseaes.2009.08.001
Yao Bochu. 1996. Tectonic evolution of the South China Sea in Cenozoic. Marine Geology & Quaternary Geology (in Chinese), 16(2): 1–13
Yao Weihua, Li Zhengxiang, Li Wuxian, et al. 2017. Proterozoic tectonics of Hainan Island in supercontinent cycles: New insights from geochronological and isotopic results. Precambrian Research, 290: 86–100, doi: 10.1016/j.precamres.2017.01.001
Yu Jinhai, O'Reilly S Y, Zhou Meifu, et al. 2012. U-Pb geochronology and Hf-Nd isotopic geochemistry of the Badu Complex, Southeastern China: Implications for the Precambrian crustal evolution and paleogeography of the Cathaysia Block. Precambrian Research, 222–223: 424–449
Yui T F, Maki K, Lan C Y, et al. 2012. Detrital zircons from the Tananao metamorphic complex of Taiwan: Implications for sediment provenance and Mesozoic tectonics. Tectonophysics, 541–543: 31–42
Zhou Di, Sun Zhen, Chen Hanzong, et al. 2008. Mesozoic paleogeography and tectonic evolution of South China Sea and adjacent areas in the context of Tethyan and Paleo-Pacific interconnections. Island Arc, 17(2): 186–207, doi: 10.1111/j.1440-1738.2008.00611.x
Zhou Xinmin, Li Wuxian. 2000. Origin of Late Mesozoic igneous rocks in southeastern China: implications for lithosphere subduction and underplating of mafic magmas. Tectonophysics, 326(3–4): 269–287
Zhou Xinmin, Sun Tao, Shen Weizhou, et al. 2006. Petrogenesis of Mesozoic granitoids and volcanic rocks in South China: A response to tectonic evolution. Episodes, 29(1): 26–33, doi: 10.18814/epiiugs/2006/v29i1/004
Zhu Weilin, Xie Xinong, Wang Zhenfeng, et al. 2017. New insights on the origin of the basement of the Xisha Uplift, South China Sea. Science China: Earth Sciences, 60(12): 2214–2222, doi: 10.1007/s11430-017-9089-9